Pergamon

*Int. J. Solids Structures* Vol. 35, No. 13, pp. 1425–1449, 1998
© 1998 Elsevier Science Ltd
All rights reserved. Printed in Great Britain
0020-7683/98 $19.00 + .00

PII: S0020-7683(97)00115-7

# SHEAR WAVES IN FIBER-REINFORCED COMPOSITES WITH INTERFACIAL CRACKS

WENLUNG LIU and RONALD D. KRIZ
Engineering Science and Mechanics Department, Virginia Polytechnic Institute and State University, Blacksburg, VA 24061-0219, U.S.A.

(*Received* 22 *October* 1996; *in revised form* 24 *March* 1997)

**Abstract**—An ensemble-average statistical method is used to calculate the overall effective mechanical properties of fiber-reinforced composites with interfacial cracks. The cracks here are specifically the fiber-matrix interfacial cracks which occur during the manufacturing process or are from inherent material defects. The problem starts with the establishment of the Helmholtz equations and boundary conditions followed by a full scale solution of the multiple scattering equations. Then by considering the low frequencies limit and the statistics of randomly spatial distribution of the fibers, a manageable homogeneous linear matrix equation is obtained. In a homogenized point of view the macroscopic mechanical properties of the composite system are derived. The calculated average mechanical properties include the overall effective shear modulus $\mu$, the average shear wave phase speed $B$, and the average specific damping capacity $\Psi$ of the composite system. The shear modulus corresponds to the elasticity of the static state, while the shear wave phase speed and damping capacity correspond to the viscoelasticity of the dynamic state of the composite. The results show that, among others:

1. the fiber-reinforced composites with interfacial cracks are transversely anisotropic material systems possessing viscoelastic behavior
2. the axially shear modulus of the composite, as the half crack length ($\delta$) increases, is in a 'decreasing steps' fashion for which finite numerical jumps exist between those steps
3. for a fiber-reinforced composite with interfacial cracks, the composite system with $1/2\pi$ half crack length is the least attenuated and is nearly transversely isotropic
4. the composite is a non-dispersed material system in low frequency ranges. © 1998 Elsevier Science Ltd.

## 1. BACKGROUND

Wave propagation methods, among others, can be used to calculate the mechanical properties of a composite. The fiber distribution of a fiber-reinforced composite is either periodic or non-periodic. In our study, we concentrate on the cases where the fiber distribution is non-periodic and random. For random distributions, many studies have contributed to the calculation of a composite's effective overall mechanical properties by the use of the multiple wave scattering method combined with the statistical-average technique. (Bose and Mal, 1973; Bose and Mal, 1974; Datta *et al.*, 1984; Yang and Mal, 1994). These models assumed perfect bonds between the fiber and matrix. Theories for waves in a variety of debonded situations have also been studied extensively. Waves in materials with interfacial cracks between two different phases are of interest in many applications, e.g., welding, nondestructive evaluation (NDE) and earthquake studies. Solution techniques include an integral equation method (Krenk and Schmidt, 1982; Neerhoff, 1979; Angel, 1988) and a perturbation method (Coussy, 1984; Coussy, 1986a). A more straightforward approach by Yang and Norris (1991) is the employment of the Helmholtz equations and Bessel functions subjected to the relevant boundary conditions. Elastic wave propagation in composites with the presence of imperfect bonding has been studied by many researchers, with various solution techniques and points of emphasis (Angel and Koba, 1993; Aboudi, 1988; Mal *et al.*, 1991; Coussy, 1986b).

In this study, we adopt the method used by Bose and Mal (1973) combined with the approach by Yang and Norris (1991) in dealing with the bonding situations. For simplicity, we assume an idealistic situation where all fibers in a composite have the same radius and bonding situation. The bonding situation is determined by the half crack length, $\delta$, and the

orientation, $\alpha$, of the crack face. For a more realistic composite, not only the fibers are distributed statistically in space. The crack for each fiber, for a damaged composite, is also statistically distributed but crack orientation, $\alpha$, is maintained. It will be more mathematically involved if the crack distribution is considered for our case and will be studied in the future. The approach we use is straightforward but mathematically rigorous. Starting with the series solutions, i.e., the Bessel functions, of the wave equation, we seek to obtain the scattering coefficients as functions of the geometrical and crack parameters and as the dynamic response of the waves in the composite. The scattering coefficients thus obtained are functions of themselves and of all the parameters involved. By performing the asymptotic analyses and, through the statistical averaging procedures, assuming the existence of an effective plane wave, a system of simultaneous linear equations emerges. Both the static property (shear modulus $\mu$) and the dynamic properties (shear wave phase velocity $B$ and specific damping capacity $\Psi$, a measurement of waves attenuation) can be deduced from this matrix equation. The average properties thus obtained are generally complex numbers for the dynamic case and real numbers for the static case. For the dynamic case, the complex numbers of the mechanical properties correspond to the viscoelasticity of the material. And the real numbers for the static case correspond to the elasticity of the material.

## 2. BOUNDARY VALUE PROBLEM

### 2.1. *Single fiber scattering*

Consider a matrix-single-fiber composite where the interface of the fiber and the matrix has a debonded crack length of $2\delta_i$ radians. The center line of the fiber crack face has an orientation of angle of $\varphi_i$ radians away from the horizontal radius line of the fiber as shown in Fig. 1. The location of the fiber '$i$' and a field point of interest as referenced to the center of the fiber are expressed by the polar coordinate system. The radius of the fiber is '$a$'. Throughout this study, the material properties associated with the matrix will be denoted as '1', and those associated with the fiber will be denoted as '2'.

Let an antiplane plane shear displacement wave, $e^{ik_1(x\cos\theta_0+y\sin\theta_0)}$, be incident upon the composite. The shear incident wave is time harmonic with a frequency of $\omega$. The time factor, $e^{-i\omega t}$, will be omitted because of the steady state of the dynamics. Then the displacement both in the matrix and in the fiber can be written as

$$u_i = \begin{cases} u^{in} + u_{1,i}, & r_i > a \\ u_{2,i}, & r_i < a \end{cases} \tag{1}$$

where $u^{in}$ is the incident wave, $u_{1,i}$ is the scattering wave in the matrix from the fiber $i$, and

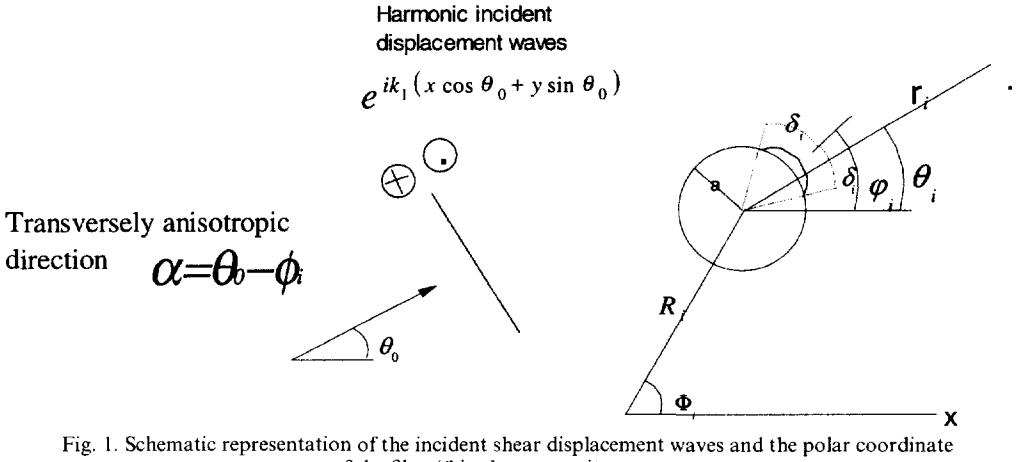


Fig. 1. Schematic representation of the incident shear displacement waves and the polar coordinate of the fiber '$i$' in the composite system.

$u_{2,i}$ is the scattering wave inside the fiber. The incident wave, $u^{in}$, and the scattering wave, $u_{1,i}$ and $u_{2,i}$, are solutions of Helmholtz equation:

$$\nabla^2 u_i + k^2 u_i = 0.$$

They can be expressed as the series representation of Bessel and Hankel functions:

$$u^{in} = e^{ik_1 R_i \cos(\Phi_i - \theta_0)} \sum_{m=-\infty}^{\infty} i^m J_m(k_1 r_i) e^{im(\theta_i - \theta_0)}$$

$$u_{1,i} = \sum_{m=-\infty}^{\infty} A_{mi} H_m(k_1 r_i) e^{im(\theta_i - \theta_0)}$$

$$u_{2,i} = \sum_{m=-\infty}^{\infty} B_{mi} J_m(k_2 r_i) e^{im(\theta_i - \theta_0)}. \tag{2}$$

In eqn (2), $k_1$ is the wave number in the matrix, $k_2$ in the fiber. The coordinate system $(r_i, \theta_i)$ is referred to the center of the fiber $i$. Note that $k_1 = \omega/\beta_1$, $k_2 = \omega/\beta_2$, $\beta_1 = \sqrt{\mu_1/\rho_1}$, $\beta_2 = \sqrt{\mu_2/\rho_2}$ where $\beta$ is the wave speed, $\mu$ is the shear modulus and $\rho$ is the material density. From the stress boundary condition on the matrix-fiber interface:

$$\mu_1 \frac{\partial}{\partial r_i}(u^{in} + u_{1,i})_{r_i = a} = \mu_2 \frac{\partial}{\partial r_i}(u_{2,i})_{r_i = a}. \tag{3}$$

Substitute the relevant terms into the above and simplify,

$$e^{ik_1 R_i \cos(\Phi_i - \theta_0)} i^n \mu_1 k_1 J_n'(k_1 a) + A_{ni} \mu_1 k_1 H_n'(k_1 a) = B_{ni} \mu_2 k_2 J_n'(k_2 a). \tag{4}$$

For displacement boundary conditions:

$$\begin{cases} (u^{in} + u_{1,i} - u_{2,i})_{r_i = a} = \Delta U_i, & -\delta_i + \varphi_i < \theta_i < \delta_i + \varphi_i \\ (u^{in} + u_{1,i} - u_{2,i})_{r_i = a} = 0, & \text{other} \end{cases} \tag{5}$$

where $\Delta U_i$ is the dynamic crack opening displacement (COD) of fiber $i$. From elasticity, the COD must be satisfied by the crack edge condition. Let $x$ be the amount of radians of angle measured from the center line of the crack face, $x$ being positive if it is measured counterclockwise, negative otherwise. Thus from Fig. 1, $x = 0$ corresponds to the center line of the crack face, $x = \pm 1$ to the broken lines indicated. Obviously, $x$ can be expressed as $x = \theta_i - \varphi_i/\delta_i$. It can be shown (Neerhoff, 1979) that the order of magnitude COD around the crack edge decreases proportionally as $O(\varepsilon^{1/2})$, where $1 - |x| \to \varepsilon$. Apparently $\varepsilon$ denotes the proportion of crack arc distances from some point to the edge of the crack. Since the Chebychev functions of the second kind $V_n(x)$ (see Appendix A) decrease proportionally as $O(\varepsilon^{1/2})$ when $1 - |x| \to \varepsilon$, i.e., when near the crack tip, it is reasonable to use $V_n(x)$ as our base function for the series expansion of COD. The COD, $\Delta U_i(\theta_i)$, can then be expressed as

$$\Delta U_i(\theta_i) = \sum_{n=1}^{\infty} \beta_{n,i} \phi_{n,i}(\theta_i) \tag{6}$$

where $\beta_{n,i}$ is the coefficient of the COD series and

$$\phi_{n,i}(\theta_i) = \frac{1}{n} V_n\left(\frac{\theta_i - \varphi_i}{\delta_i}\right) = \frac{1}{n}\sin\left(\frac{n\pi}{2} - n\sin^{-1}\frac{\theta_i - \varphi_i}{\delta_i}\right), \quad n = 1, 2, 3 \ldots \tag{7}$$

Substitute the relevant terms into the displacement boundary condition and simplify

$$e^{ik_1 R_i \cos(\Phi_i - \theta_0)} i^n J_n(k_1 a) + A_{ni} H_n(k_1 a) = B_{ni} J_n(k_2 a) + \frac{e^{in(\theta_0 - \varphi_i)}}{2n} \sum_{n'=1}^{\infty} \beta_{n',i} i^{n'+1} J_{n'}(-n\delta_i), \quad n \neq 0$$

$$e^{ik_1 R_i \cos(\Phi_i - \theta_0)} J_0(k_1 a) + A_{0i} H_0(k_1 a) = B_{0i} J_0(k_2 a) + \tfrac{1}{4}\beta_{1,i}\delta_i, \quad n = 0. \tag{8}$$

Combining eqns (4) and (8) for m $\neq$ 0 yields

$$\begin{aligned}
A_{mi} &= \frac{E_m}{D_m} F_{mi} \\
B_{mi} &= \frac{2i}{\pi k_1 a}\frac{F_{mi}}{D_m} + \frac{J'_m(k_1 a)}{2mE_m} e^{im(\theta_0 - \varphi_i)} \sum_{n'=1}^{\infty} \beta_{n',i} i^{n'+1} J_{n'}(-m\delta_i), \\
F_{mi} &= e^{ik_1 R_i \cos(\Phi_i - \theta_0)} i^m - \frac{zJ'_m(k_2 a)}{2mE_m} e^{im(\theta_0 - \varphi_i)} \sum_{n'=1}^{\infty} \beta_{n',i} i^{n'+1} J_{n'}(-m\delta_i)
\end{aligned} \tag{9}$$

and for $m = 0$,

$$\begin{aligned}
A_{0i} &= \frac{E_0}{D_0} F_{0i} \\
B_{0i} &= \frac{2i}{\pi k_1 a}\frac{F_{0i}}{D_0} + \frac{J'_0(k_1 a)}{4F_0}\beta_{1,i}\delta_i \\
F_{0i} &= e^{ik_1 R_i \cos(\Phi_i - \theta_0)} - \frac{zJ'_0(k_2 a)}{4E_0}\beta_{1,i}\delta_i
\end{aligned} \tag{10}$$

where

$$\begin{aligned}
E_m &= zJ_m(k_1 a)J'_m(k_2 a) - J_m(k_2 a)J'_m(k_1 a) \\
D_m &= J_m(k_2 a)H'_m(k_1 a) - zJ'_m(k_2 a)H_m(k_1 a) \\
z &= \frac{\mu_2 k_2}{\mu_1 k_1}.
\end{aligned}$$

The $\beta$ terms in the above equations can be solved by requiring that, at fiber $i$, the stress on the crack face is vanished. Therefore, at fiber '$i$',

$$\frac{\partial}{\partial r_i}(u_{2,i})_{r_i = a} = 0, \; -\delta_i + \varphi_i < \theta_i < \delta_i + \varphi_i. \tag{11}$$

Substituting (2) into the equation above yields

$$B_{0,i} J'_0(k_2 a)\frac{(-1)^m \pi \delta_i}{2m}\delta_{1m} = \sum_{p \neq 0}^{\infty} B_{pi} J'_p(k_2 a) e^{-ip(\theta_0 - \varphi_i)} \frac{\pi}{-p} i^{m+1} J_m(p\delta_i),$$

$$-\delta_i + \varphi_i < \theta_i < \delta_i + \varphi_i. \tag{12}$$

Substitute $B$ terms from (9) and (10) into the above equation and multiply both sides by $\phi_m(\theta_i)$, $m = 1, 2, 3 \ldots$. Integrating with respect to $\theta_i$ from $-\delta_i + \varphi_i$ to $\delta_i + \varphi_i$, we get

$$\frac{i}{\pi k_1 a} J_0'(k_2 a) \frac{(-1)^m \delta_i}{m D_0} \delta_{1m} F_{0i} + \sum_{p \neq 0}^{\infty} \frac{2i}{\pi k_1 a} J_p'(k_2 a) e^{-ip(\theta_0 - \varphi_i)} \frac{i^{m+1}}{p D_p} J_m(p\delta_i) F_{pi}$$

$$= \frac{J_0'(k_1 a)}{8E_0} \delta_i^2 J_0'(k_2 a) \frac{(-1)^{m+1}}{m} \delta_{1m} \beta_{1,i}$$

$$- \sum_{p \neq 0}^{\infty} \frac{J_p'(k_1 a) J_p'(k_2 a)}{2p^2 E_p} i^{m+1} J_m(p\delta_i) \sum_{n=1}^{\infty} \beta_{n,i} i^{n+1} J_n(-p\delta_i). \quad (13)$$

Simplify further and rearrange, and we get the matrix equation in $\beta$ as

$$[Q_{mn,i}]\{\beta_{n,i}\} = \{N_{m,i}\}$$

where

$$Q_{mn,i} = \left( \frac{iz}{\pi k_1 a} J_0'(k_2 a) \frac{(-1)^m}{D_0} + \frac{J_0'(k_1 a)}{2} (-1)^{m+1} \right) \frac{\delta_i^2}{m} \frac{J_0'(k_2 a)}{4E_0} \delta_{1m} \delta_{1n}$$

$$+ i^{n+1} \left[ J_n(-m\delta_i) \frac{-i^m}{\pi k_1 a} \frac{z J_m'(k_2 a)}{m E_m} e^{im(\theta_0 - \varphi_i)} \sum_{p \neq 0}^{\infty} J_p'(k_2 a) e^{-ip(\theta_0 - \varphi_i)} \frac{J_m(p\delta_i)}{D_p p} \right.$$

$$\left. - i^{m+1} \sum_{p \neq 0}^{\infty} \frac{J_p'(k_1 a) J_p'(k_2 a)}{2p^2 E_p} J_n(-p\delta_i) J_m(p\delta_i) \right]$$

$$N_{m,i} = \left[ J_0'(k_2 a) \frac{\delta_i}{m D_0} \delta_{1m} + \sum_{p \neq 0}^{\infty} J_p'(k_2 a) e^{-ip(\theta_0 - \varphi_i)} \frac{2i}{D_p p} J_m(p\delta_i) \right] \frac{i}{\pi k_1 a} (-1)^m e^{ik_1 p_i \cos(\Phi_i - \theta_0)}. \quad (14)$$

Note that $\delta_{mn}$'s are the Kronecker delta. The $\beta$ terms can then be solved numerically in light of the above equation. Equation (14) can be simplified further for the quasi-static case, i.e., when the wave length is large compared with the fiber radius. In this case, it is reasonable to assume that both $k_1 a$ and $k_2 a$ are small compared to 1 and that the order of $k_1 a$ and $k_2 a$ are approximately the same. Therefore if the wave length is large compared with the fiber radius,

$$Q_{mn,i} \sim i^{n+1} \left[ z J_n(-m\delta_i) J_m(\delta_i) \frac{k_1 i^{m+1} e^{im(\theta_0 - \varphi_i)} e^{-i(\theta_0 - \varphi_i)}}{k_2 \left( \frac{\mu_2}{\mu_1} - 1 \right) \left( \frac{\mu_2}{\mu_1} + 1 \right) \left( \frac{k_1 a}{2} \right)^{m-1}} \right.$$

$$\left. - \frac{i^{m+1}}{2 \left( \frac{\mu_2}{\mu_1} - 1 \right)} \sum_{p \neq 0}^{\infty} \frac{J_n(-p\delta_i) J_m(p\delta_i)}{p} \right]$$

and

$$N_{m,i} \sim \frac{i(-1)^m e^{-i(\theta_0 - \varphi_i)}}{\left( \frac{\mu_2}{\mu_1} + 1 \right)} J_m(\delta_i) e^{ik_1 R_i \cos(\Phi_i - \theta_0)} k_1 a. \quad (15)$$

It is apparent that the order of $\beta$ terms are $O(k_1 a)$ in the quasi-static case, judging from the equations above.

2.2. *Multiple wave scattering*

For a composite in which there are $N$ fibers embedded in the matrix, the effect of multiple wave scattering should be considered. The scattering coefficients $A_{mi}$ and $B_{mi}$ for a multiple scattering case in eqn (2) are the same as in the single fiber scattering one, except that $F_{mi}$ terms should include the multiple scattering effects. Thus for the multiple wave scattering case, the displacement both in the matrix and in the fibers is

$$u_i = \begin{cases} u^{in} + \sum_{i=1}^{N} u_{1,i}, & r_i > a \\ u_{2,i}, & r_i < a \end{cases}. \tag{16}$$

Introducing the stress and displacement boundary conditions for all the fibers, we have, for each fiber $i$ and if $m \neq 0$,

$$A_{mi} = \frac{E_m}{D_m} F_{mi}$$

$$B_{mi} = \frac{2i}{\pi k_1 a} \frac{F_{mi}}{D_m} + \frac{J'_m(k_1 a)}{2mE_m} e^{im(\theta_0 - \varphi_i)} \sum_{k'=1}^{\infty} \beta_{n',i} i^{n'+1} J_{n'}(-m\delta_i)$$

$$F_{mi} = e^{ik_1 R_i \cos(\Phi_i - \theta_0)} i^m - \frac{zJ'_m(k_2 a)}{2mE_m} e^{im(\theta_0 - \varphi_i)} \sum_{n'=1}^{\infty} \beta_{n',i} i^{n'+1} J_{n'}(-m\delta_i)$$

$$+ \sum_{j \neq i}^{N} \sum_{n=-\infty}^{\infty} \frac{E_{m+n}}{D_{m+n}} F_{n+n,j} e^{in(\theta_{ij} - \theta_0)} H_n(k_1 r_{ij}). \tag{17}$$

If $m = 0$,

$$A_{0i} = \frac{E_0}{D_0} F_{0i}$$

$$B_{0i} = \frac{2i}{\pi k_1 a} \frac{F_{0i}}{D_0} + \frac{J'_0(k_1 a)}{4E_0} \beta_{1,i} \delta_i$$

$$F_{0i} = e^{ik_1 R_i \cos(\Phi_i - \theta_0)} - \frac{zJ'_0(k_2 a)}{4E_0} \beta_{1,i} \delta_i + \sum_{j \neq i}^{N} \sum_{n=-\infty}^{\infty} \frac{E_n}{D_n} F_{n,j} e^{in(\theta_{ij} - \theta_0)} H_n(k_1 r_{ij}). \tag{18}$$

## 3. STATISTICAL CONSIDERATIONS

3.1. *Random distribution of the fibers*

The geometrical parameters that affect the distribution probability of the fibers in the composite consist of the number of the fibers per unit volume, $n_0$, and the radius of the fibers '$a$'. Other than these two factors, a statistical parameter, $s_i$, needs to be determined. For simplicity, the statistical distribution is only limited to the distribution of the fibers in the composite. Other parameters which in practice may be statistically distributed in the domain of interest include the half crack length, $\delta$, and the orientation, $\alpha$, of the crack face of each fiber. A mathematical model to accommodate the cracks distribution, if possible in a limited fashion, will be studied in the future. For simplicity, we assume all interfacial cracks possess the same orientations and half crack length. The following statistical treatments are similar to those in Bose and Mal (1973), except that the correlation term is defined with more explicit geometrical information.

The domain we consider is physically a three-dimensional space. But throughout this study, the derivation involves only two dimensions (polar $R-\Phi$) due to the fact that the fibers are unidirectional and that the shear component of the quantity concerned (the '$z$'

direction component) is a function of the other two coordinates. Thus vector $\mathbf{R}_i$ is appropriately regarded as $\mathbf{R}_i = (R_i, \Phi_i)$, where the polar components are in a global sense in the composite domain. For a uniform composite for which the fibers are randomly distributed in the matrix,

$$\begin{aligned} p(\mathbf{R}_1) &= p(\mathbf{R}_i), \quad 1 \leqslant i \leqslant N \\ p(\mathbf{R}_2 \mid \mathbf{R}_1) &= p(\mathbf{R}_i \mid \mathbf{R}_j), \quad 1 \leqslant i,j \leqslant N, \quad i \neq j \\ p(\mathbf{R}_1, \mathbf{R}_2, \ldots, \mathbf{R}_N) &= p(\mathbf{R}_1) p(\mathbf{R}_2, \mathbf{R}_3, \ldots, \mathbf{R}_N \mid \mathbf{R}_1) \\ &= p(\mathbf{R}_1) p(\mathbf{R}_2 \mid \mathbf{R}_1) p(\mathbf{R}_3, \mathbf{R}_4, \ldots, \mathbf{R}_N \mathbf{R}_1, \mathbf{R}_2). \end{aligned} \tag{19}$$

The first equation of (19) states that the probability that a fiber is located at $\mathbf{R}_i$ is equally probable for all randomly distributed fibers within the domain of the composite. The second equation states that the conditional probability for any two concerned fibers is all the same. The third equation is a generalized expansion of the joint probability of all the fibers concerned. Therefore, as the probability density is normalized and the area occupied by a fiber is neglected in a sufficiently large domain, $p(\mathbf{R}_i)$ should be equal to $1/s$, where $s$ is the cross sectional area of the composite domain. For definiteness, we have

$$\int_v p(\mathbf{R}_i)\, \mathrm{d}\tau_i = \int_v \frac{1}{s} \mathrm{d}\tau_i = \frac{1}{s} \int_v \mathrm{d}\tau_i = \frac{1}{s} \times s = 1. \tag{20}$$

The above equation states, indeed, that the probability that a fiber $i$ exists in the composite domain is equal to 1.

3.2. *Simulation of the correlation function*

Considering the conditional probability $p(\mathbf{R}_2 \mid \mathbf{R}_1)$. For $r_{12}$ (the distance between fiber 1 and fiber 2) $\to \infty$, the probability that fiber 2 exists at an infinite distance away from fiber 1 is the same as the probability that any single fiber exists in the composite without considering any other fibers, which is $1/s$. Yet for $r_{12} \leqslant 2a$, $p(\mathbf{R}_2 \mid \mathbf{R}_1) = 0$ because of the non-penetration condition of fibers. For the case where the fiber radius is smaller and the number of fibers per unit volume $n_0$ larger, it is more likely to find another fiber at a given distance away from an existing fiber. This corresponds to the steeper slope of the correlation curve in Fig. 2. Accordingly, the correlation probability $p(\mathbf{R}_2 \mid \mathbf{R}_1)$ can be simulated as an exponential function of $r_{12}$. Thus

$$\begin{aligned} p(\mathbf{R}_2 \mid \mathbf{R}_1) &= \frac{1}{s}(1 - f(r_{12})), \quad r_{12} > 2a \\ &= 0, \quad r_{12} \leqslant 2a \end{aligned}$$

where $f(r_{12}) = \mathrm{Re}^{-r_{12}/(a/n_0)^{s_i}}$, $0 < R < e^{2a/(a/n_0)^{s_i}}$.

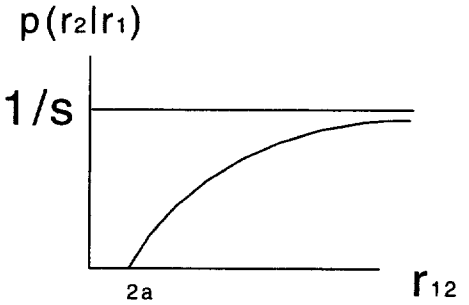


Fig. 2. Simulation of the correlation function.

The above is usually referred to as 'well-stirred' approximation (Datta *et al.*, 1984) which is not valid for high concentration of scatterers. For a large sample, or for a large domain of the composite, $R \to e^{2a/(a/n_0)^{s_i}}$ due to the fact that the number of fibers surrounding the existing fiber is small compared with '$N$', the number of fibers in the composite. Note that the statistical parameter '$s_i$' needs to be determined statistically. Finally the normalization requires that

$$\lim_{R\to\infty} \frac{1}{R^2} \int_{2a}^{R} f(r_{12}) r_{12}\, \mathrm{d}r_{12} = 0.$$

## 4. AVERAGING TECHNIQUE

### 4.1. *Indistinguishability of fibers and quasi-crystalline approximation*

From the third equation of (17) and that of (18), $F_{mi}$ is a function of $\beta$ terms and themselves, in addition to the geometrical information and the dynamic input of the composite system. It contains the scattering information associated with each fiber '$i$' and the geometrical relations with all the fibers other than fiber '$i$'. Therefore, it is the quantity on which we perform the averaging process in order to gain an overall effective material property for the composite system. The rationale for performing the averaging process is based on the fact that (1) all the fibers are indistinguishable from a random point of view, as stated in the first two equations of (19); (2) the multiple scattering in the composite system is the dual combination of the coherent waves and incoherent waves. Apparently, the averaging material property is the overall effective quantity due to the coherent waves. And the coherent waves in the composite are the non-constructive part of the multiple scattering waves in the composites. Throughout this study, elasticity is the only mechanism involved before the averaging process is performed. After the averaging process, the contribution from the incoherent waves is lost in the calculation of the effective property of the composite. Hence, the viscoelasticity emerges as the end result to reflect the fact that part of the multiple scattering energy, i.e., those of the non-coherent waves, is lost.

Therefore due to the indistinguishability of the fibers, one can choose any fiber to investigate the expectation value of $F_{mi}$ without loss of generality. Thus, for fiber '1',

$$\begin{aligned} F_{m1} &= e^{ik_1 R_1 \cos(\Phi_1 - \theta_0)} i^m - \frac{zJ'_m(k_2 a)}{2mE_m} e^{im(\theta_0 - \varphi_1)} \sum_{n=1}^{\infty} \beta_{n,1} i^{n+1} J_n(-m\delta_1) \\ &\quad + \sum_{j=2}^{N} \sum_{n=-\infty}^{\infty} \frac{E_{m+n}}{D_{m+n}} F_{n+m,j} H_n(k_1 r_{1j})\, e^{in(\theta_{1j} - \theta_0)}, \quad m \neq 0 \\ F_{01} &= e^{ik_1 R_1 \cos(\Phi_1 - \theta_0)} - \frac{zJ'_0(k_2 a)}{4E_0} \beta_{1,1} \delta_1 \\ &\quad + \sum_{j=2}^{N} \sum_{n=-\infty}^{\infty} F_{n,j} H_n(k_1 r_{1j})\, e^{in(\theta_{1j} - \theta_0)}. \end{aligned} \tag{21}$$

First, take the conditional expectation value of $F_{m1}$, i.e., $\langle F_{m1} \rangle_1$, in light of eqn (21). The conditional expectation value of a function $f$ is defined as

$$\begin{aligned} \langle f \rangle_1 &= \int \cdots \int_v f p(\mathbf{R}_2 \cdots \mathbf{R}_n \mid \mathbf{R}_1)\, \mathrm{d}\tau_2 \cdots \mathrm{d}\tau_n \\ \langle f \rangle_{12} &= \int \cdots \int_v f p(\mathbf{R}_3 \cdots \mathbf{R}_n \mid \mathbf{R}_1, \mathbf{R}_2)\, \mathrm{d}\tau_3 \cdots \mathrm{d}\tau_n \end{aligned} \tag{22}$$

where $\langle f \rangle_1$ is when the information (location in our case) of scatterer '1' is given, and $\langle f \rangle_{12}$

is when the information of scatterers '1' and '2' are given. Using eqn (22) and the correlation probability defined in the 'well-stirred' approximation, (21) becomes

$$\langle F_{m1}\rangle_1 = e^{ik_1R_1\cos(\Phi_1-\theta_0)}i^m - \frac{zJ'_m(k_2a)}{2mE_m}e^{im(\theta_0-\varphi_1)}\sum_{n=1}^{\infty}\langle\beta_{n,1}\rangle_1 i^{n+1}J_n(-m\delta_1)$$

$$+n_0\sum_{n=-\infty}^{\infty}\frac{E_{m+n}}{D_{m+n}}\int_{|\bar r_2-\bar r_1|\geq 2a}(1-e^{2a-r_{12}/(a/n_0)^{y_1}})\langle F_{n+m,2}\rangle_2 H_n(k_1r_{12})\,e^{in(\theta_{12}-\theta_0)}\,d\tau_2, \quad m\neq 0$$

$$\langle F_{01}\rangle_1 = e^{ik_1R_1\cos(\Phi_1-\theta_0)} - \frac{zJ'_0(k_2a)}{4E_0}\langle\beta_{1,1}\rangle_1\delta_1$$

$$+n_0\sum_{n=-\infty}^{\infty}\frac{E_n}{D_n}\int_{|\bar r_2-\bar r_1|\geq 2a}(1-e^{2a-r_{12}/(a/n_0)^{y_1}})\langle F_{n,2}\rangle_2 H_n(k_1r_{12})\,e^{in(\theta_{12}-\theta_0)}\,d\tau_2. \quad (23)$$

In obtaining the above equations, the indistinguishable property of (19) is again used for the third term of the right hand side of both equations in (21). In addition, the quasi-crystalline approximation

$$\langle F_{mi}\rangle_{ij} = \langle F_{mi}\rangle_i, \quad i\neq j$$

is employed and a large sample condition is considered.

4.2. *Extinction theory*

The extinction theorem states that the incident wave is vanished upon entering the composite (Bose and Mal, 1973), or that the incident wave is canceled by waves generated at the boundary (Waterman and Truell, 1961). By applying this theorem, we appeal to the physics, not the mathematics, of eqn (23). The setup of the boundary value problem at the beginning of this treatment is the initial step for gaining the multiple scattering information inherited by the presence of the fibers and cracks. Once the scattering formula is established (eqns 17 and 18), statistical-averaging techniques need to be introduced to obtain the overall effective property of the composite system. By doing this, the energy of incident waves is assumed to 'transform' to the scattering waves in the system and all the scattering waves traveling to the infinite boundary of the system are canceled by the incident wave. Thus in eqn (23) the quantities associated with the infinite boundary of the composite, i.e. the upper limit of the integral term on the right hand side of both equations, are canceled by the incident wave. Finally assuming the existence of an average wave such that $\langle F_{mi}\rangle_i = i^mF_m\,e^{iKR_i\cos(\Phi_i-\theta_0)}$, where $K$ represents the overall effective wave number in the composite system, eqn (23) then becomes

$$i^mF_m\,e^{iKR_1\cos(\Phi_1-\theta_0)} \sim \frac{-zJ'_m(k_2a)}{2mE_m}e^{im(\theta_0-\varphi_1)}\sum_{n=1}^{\infty}\langle\beta_{n,1}\rangle_1 t^{n+1}J_n(-m\delta_1)$$

$$+2\pi n_0\,e^{iKR_1\cos(\Phi_1-\theta_0)}i^m\sum_{n=-\infty}^{\infty}\frac{E_{m+n}}{D_{m+n}}F_{n+m}\left[\frac{a}{k_1^2-K^2}\left(J_n(2Ka)\frac{\partial}{\partial a}H_n(2k_1a)\right.\right.$$

$$\left.\left.-H_n(2k_1a)\frac{\partial}{\partial a}J_n(2Ka)\right)-\int_{2a}^{0}e^{2a-r_{12}/(a/n_0)^{y_1}}J_n(Kr_{12})H_n(k_1r_{12})r_{12}\,dr_{12}\right], \quad m\neq 0$$

$$F_0\,e^{iKR_1\cos(\Phi_1-\theta_0)} \sim \frac{-zJ'_0(k_2a)}{4E_0}\delta_1/\beta_{1,1}\rangle_1$$

$$+2\pi n_0\,e^{iKR_1\cos(\Phi_1-\theta_0)}\sum_{n=-\infty}^{\infty}\frac{E_n}{D_n}F_n\left[\frac{a}{k_1^2-K^2}\left(J_n(2Ka)\frac{\partial}{\partial a}H_n(2k_1a)\right.\right.$$

$$\left.\left.-H_n(2k_1a)\frac{\partial}{\partial a}J_n(2Ka)-\int_{2a}^{0}e^{2a-r_{12}/(a/r_0)^{y_1}}J_n(Kr_{12})H_n(k_1r_{12})r_{12}\,dr_{12}\right]\right. \quad (24)$$

## 5. CONSTRUCTION OF THE LINEAR SYSTEM OF EQUATIONS

### 5.1. *Asymptotic analyses*

If eqn (24) is to be mathematically manageable an asymptotic analysis is desired. We resort to the fact that, for wave length large compared to the radius of the fiber (low frequencies waves), the Bessel functions can be approximated as a power order of $k_i a$, $i = 1, 2$. Therefore by approximating the Bessel functions in the low frequencies regime, the $F$ terms are assumed, based on eqn (24), to have order of $F_0 \sim O(k_1 a)^{t-1}$ and $F_m \sim O(k_1 a)^{t-|m|}$, where $t$ is 1 according to eqn (15) for the order of the quantity of $\beta$ terms. The statistical average of $\beta$ terms in (24) can be obtained by requiring that the stress on the crack face of each fiber is vanished. Thus bear in mind that in using equation (13) for the vanished stress on the crack face, the $F$ terms are referred to as in equations (17) and (18) for the multiple scattering case. Performing the low frequencies analysis on (13) and considering the order of magnitude of the $F$ terms in the previous statement, we get

$$\sum_{n=1}^{\infty}\sum_{p=1}^{\infty}\frac{J_m(p\delta_i)J_n(p\delta_i)}{p} i^{n+1}((-1)^m+(-1)^n)\beta_{n,i} = 4\frac{\mu_2-\mu_1}{\mu_2+\mu_1}\sum_{p=1}^{\infty}\frac{J_m(p\delta_i)}{p!}\left(\frac{k_1 a}{2}\right)^p((1-1)^{p+m}e^{ip\alpha}F_{-pi}-e^{-ip\alpha}F_{pi}). \quad (25)$$

Note that in obtaining (25), $\alpha = \theta_0 - \varphi_i$ (defined as the transversely anisotropic direction) in the above equation and the first term on the left and right hand side of (13) are neglected. Equation (25) can be rewritten as $[Q_{mn,i}]\{\beta_{n,i}\} = \{N_{m,i}\}$ where

$$Q_{mn,i} = i^{n+1}[(-1)^m+(-1)^n]\sum_{p=1}^{\infty}\frac{J_m(p\delta_i)J_n(p\delta_i)}{p}$$

$$N_{m,i} = 4\frac{\mu_2-\mu_1}{\mu_2+\mu_1}\sum_{p=1}^{\infty}\frac{J_m(p\delta_i)}{p!}\left(\frac{k_1 a}{2}\right)^p[(-1)^{p+m}e^{ip\alpha}F_{-pi}-e^{-ip\alpha}F_{pi}]. \quad (26)$$

Take the conditional statistical average of the above equation and consider the fact that $\langle F_{pi}\rangle_i = i^p F_p e^{iKR_i\cos(\Phi_i-\theta_0)}$, yields

$$\langle\beta_{n,i}\rangle_i = \sum_{p=1}^{\infty}\left(\sum_{m=1}^{\infty}q_{nm,i}X_{mp}\right)i^{-p}F_{-p}e^{iKR_i\cos(\Phi_i-\theta_0)}(k_1 a)^p + \sum_{p=1}^{\infty}\left(\sum_{m=1}^{\infty}q_{nm,i}Y_{mp}\right)i^p F_p e^{iKR_i\cos(\Phi_i-\theta_0)}(k_1 a)^p \quad (27)$$

where

$$[q_{nm,i}] = [Q_{mn,i}]^{-1}$$

$$X_{mp} = 4\frac{\mu_2-\mu_1}{\mu_2+\mu_1}\frac{J_m(p\delta_i)}{p!2^p}(-1)^{p+m}e^{ip\alpha}$$

$$Y_{mp} = 4\frac{\mu_2-\mu_1}{\mu_2+\mu_1}\frac{J_m(p\delta_i)}{p!2^p}(-1)e^{-ip\alpha}. \quad (28)$$

It will be beneficial, as will be seen later, to transform the $F$ terms to a new set of quantities. That is, we let

$$\bar{F}_0 = F_0 \times (k_1 a) \sim O(k_1 a)^t$$
$$\bar{F}_p = F_p \times (k_1 a)^p \sim O(k_1 a)^t$$
$$\bar{F}_{-p} = F_{-p} \times (k_1 a)^p \sim O(k_1 a)^t.$$

Note that '$p$' in the above equation is a positive integer. Thus the orders of the $\bar{F}$ terms are asymptotically the same and (27) becomes

$$\langle \beta_{n,i} \rangle_i = \sum_{p=1}^{\infty} \left( \sum_{m=1}^{\infty} q_{nm,i} X_{mp} \right) i^{-p} \bar{F}_{-p} e^{iKR_i \cos(\Phi_i - \theta_0)} + \sum_{p=1}^{\infty} \left( \sum_{m=1}^{\infty} q_{nm,i} Y_{mp} \right) i^p \bar{F}_p e^{iKR_i \cos(\Phi_i - \theta_0)} (k_1 a)^p. \quad (29)$$

Substituting (29) to (24) and considering the low frequencies limit, we get a homogeneous linear equations in $\bar{F}$. For $m \geqslant 2$,

$$\bar{F}_{-m} = \frac{z e^{-im\alpha} (-i)^m}{(m-1)! \left( \frac{\mu_2}{\mu_1} - 1 \right)} \frac{k_1}{k_2} 2^{m-1} \sum_{n=1}^{\infty} \left\{ \sum_{p=1}^{\infty} \left( \sum_{m'=1}^{\infty} q_{nm',i} X_{m'p} \right) i^{-p} \bar{F}_{-p} + \sum_{p=1}^{\infty} \left( \sum_{m'=1}^{\infty} q_{nm',i} Y_{m'p} \right) i^p \bar{F}_p \right\} i^{n+1} J_n(m\delta_i),$$

$$\bar{F}_m = \frac{-z e^{im\alpha} i^{-m}}{(m-1)! \left( \frac{\mu_2}{\mu_1} - 1 \right)} \frac{k_1}{k_2} 2^{m-1} \sum_{n=1}^{\infty} \left\{ \sum_{p=1}^{\infty} \left( \sum_{m'=1}^{\infty} q_{nm',i} X_{m'p} \right) i^{-p} \bar{F}_{-p} + \sum_{p=1}^{\infty} \left( \sum_{m'=1}^{\infty} q_{nm',i} Y_{m'p} \right) i^p \bar{F}_p \right\} i^{n+1} J_n(m\delta_i)(-1)^n. \quad (30)$$

In obtaining the above equation, the positive and negative of $m$ in the first equation of (24) need to be considered separately. Also note that the second term of the right hand side of both equations in (24) is neglected in obtaining (30). For $m = 1$,

$$\frac{-z e^{-i\alpha}}{\left( \frac{\mu_2}{\mu_1} - 1 \right)} \frac{k_1}{k_2} \sum_{n=1}^{\infty} \sum_{p=2}^{\infty} \left( \sum_{m'=1}^{\infty} q_{mn',i} X_{m'p} \right) i^{n-p} \bar{F}_{-p} J_n(\delta_i)$$
$$+ \left[ \frac{cu_1}{1 - \left( \frac{K}{k_1} \right)^2} + 1 + \frac{\pi i}{2} cu_1 J_0 - \frac{z e^{-i\alpha}}{\left( \frac{\mu_2}{\mu_1} - 1 \right)} \frac{k_1}{k_2} \sum_{n=1}^{\infty} \left( \sum_{m'=1}^{\infty} q_{mn',i} X_{m'1} \right) i^{n-1} J_n(\delta_i) \right] \bar{F}_{-1}$$
$$+ \left[ \frac{cu_0}{1 - \left( \frac{K}{k_1} \right)^2} \frac{K}{k_1} + \frac{\pi i}{2} cu_0 I_1 \right] \bar{F}_0 + \left[ \frac{cu_1}{1 - \left( \frac{K}{k_1} \right)^2} \left( \frac{K}{k_1} \right)^2 + \frac{\pi i}{2} cu_1 I_2 \right]$$

$$-\frac{ze^{-i\alpha}}{\left(\frac{\mu_2}{\mu_1}-1\right)}\frac{k_1}{k_2}\sum_{n=1}^{\infty}\left(\sum_{m'=1}^{\infty}q_{nm',i}Y_{m'1}\right)i^{n+1}J_n(\delta_i)\Bigg]\bar{F}_1$$

$$+\frac{-ze^{-i\alpha}}{\left(\frac{\mu_2}{\mu_1}-1\right)}\frac{k_1}{k_2}\sum_{n=1}^{\infty}\sum_{p=2}^{\infty}\left(\sum_{m'=1}^{\infty}q_{nm',i}Y_{m'p}\right)i^{n+p}\bar{F}_pJ_n(\delta_i)=0. \tag{31}$$

For $m = 0$, the first term in the second equation of (24) is neglected, therefore

$$\left[\frac{cu_1}{1-\left(\frac{K}{k_1}\right)^2}\left(\frac{K}{k_1}\right)+\frac{\pi i}{2}cu_1I_1\right]\bar{F}_{-1}+\left[\frac{cu_0}{1-\left(\frac{K}{k_1}\right)^2}+1+\frac{\pi i}{2}cu_0I_0\right]\bar{F}_0$$

$$+\left[\frac{cu_1}{1-\left(\frac{K}{k_1}\right)^2}\left(\frac{K}{k_1}\right)+\frac{\pi i}{2}cu_1I_1\right]\bar{F}_1=0. \tag{32}$$

For $m = 1$,

$$\frac{ze^{i\alpha}}{\left(\frac{\mu_2}{\mu_1}-1\right)}\frac{k_1}{k_2}\sum_{n=1}^{\infty}\sum_{p=2}^{\infty}\left(\sum_{m'=1}^{\infty}q_{nm',i}X_{m'p}\right)i^{n-p}\bar{F}_{-p}J_n(\delta_i)(-1)^n$$

$$+\left[\frac{cu_1}{1-\left(\frac{K}{k_1}\right)^2}\left(\frac{k_1}{k_2}\right)^2+\frac{\pi i}{2}cu_1I_2+\frac{ze^{i\alpha}}{\left(\frac{\mu_2}{\mu_1}-1\right)}\frac{k_1}{k_2}\right.$$

$$\left.\times\sum_{n=1}^{\infty}\left(\sum_{m'=1}^{\infty}q_{nm',i}X_{m'1}\right)i^{n-1}J_n(\delta_i)(-1)^n\right]\times\bar{F}_{-1}+\left[\frac{cu_0}{1-\left(\frac{K}{k_1}\right)^2}\frac{K}{k_1}+\frac{\pi i}{2}cu_0I_1\right]\bar{F}_0$$

$$+\left[\frac{cu_1}{1-\left(\frac{K}{k_1}\right)^2}+1+\frac{\pi i}{2}cu_1I_0+\frac{ze^{i\alpha}}{\left(\frac{\mu_2}{\mu_1}-1\right)}\frac{k_1}{k_2}\sum_{n=1}^{\infty}\left(\sum_{m'=1}^{\infty}q_{nm',i}Y_{m'1}\right)i^{n+1}J_n(\delta_i)(-1)^n\right]\bar{F}_1$$

$$+\frac{ze^{i\alpha}}{\left(\frac{\mu_2}{\mu_1}-1\right)}\frac{k_1}{k_2}\sum_{n=1}^{\infty}\sum_{p=2}^{\infty}\left(\sum_{m'=1}^{\infty}q_{nm',i}Y_{m'p}\right)i^{n+p}\bar{F}_pJ_n(\delta_i)(-1)^n=0. \tag{33}$$

Note that in (31), (32) and (33)

$$c=\pi a^2n_0$$

$$u_0=\frac{\rho_2}{\rho_1}-1$$

$$u_1 = \frac{1-\mu_2/\mu_1}{1+\mu_2/\mu_1}$$

$$I_n = \int_{2k_1 a}^{0} e^{2a-(x/k_1)/(a/n_0)^{s_1}} J_n\left(\frac{K}{k_1}x\right) H_n(x)x\,\mathrm{d}x, \quad n = 0, 1, 2. \tag{34}$$

The $I_n$ terms in the above equation must have magnitude of order equal to or less than $O(1)$ in order for the asymptotic analyses to be applicable. Thus eqns (30), (31), (32), (33) form a homogeneous linear equation system in $\bar{F}$. By stipulating that the coefficients of $\bar{F}$ terms form a linear matrix and that the determinant of the matrix is equal to zero, the quantity of $K/k_1$ can be evaluated.

5.2. *Computational technique*

The determinant formed previously, by performing column and row operations (addition, subtraction and multiplication) for the elements of the determinant, a simple equation emerges as the following:

$$\left(\frac{K}{k_1}\right)^2 = 1 + cu_0 + (cu_1 + cu_0 cu_1)\frac{\begin{vmatrix} a_{11} & a'_{12} \\ a'_{21} & a'_{22} \end{vmatrix}}{\begin{vmatrix} a_{11} & a_{12} \\ a_{21} & a_{22} \end{vmatrix}}. \tag{35}$$

The numerator of the right-hand side of the above equation is a $(2m-1)\times(2m-1)$ determinant and the denominator is a $(2m\times 2m)$ determinant. More specifically, the $a$'s in the above are all sub-elements structure (see Appendix B for the list of $a$'s). The overall effective wave number $K$ in eqn (35) is a complex number, i.e.,

$$K = \mathrm{Re}(K) + i\,\mathrm{Im}(K)$$

where $\mathrm{Re}(K) = \omega/B$, and $B$ is the overall effective shear wave phase speed in the composite. Note that a measurement of wave attenuation in the composite is the specific damping capacity, which is defined as $\Psi = 4\pi(\mathrm{Im}(K)/\mathrm{Re}(K))$.

A Fortran program was written to perform the computation of $(K/k_1)^2$ in (35). For the static case, the probability correlation terms $I_n$ are vanished. The normalized wave number (with respect to the material property of matrix) in (35) can be transformed to obtain the normalized shear modulus. The double summation in the computation of elements of $a$'s (Appendix B) needs to be carried out for the same number of terms (for our case, we give each summation 30 terms). And for the $Q$'s terms in (26) to be definite, ten-thousand terms are used for the case where the crack length is larger than 0.01 degrees. For crack lengths less than or equal to 0.01, we resort to the analytic calculation which follows.

When $\delta$ is small ($\delta \leqslant 0.01$) the summation of $Q$ terms in the second equation of (26) can be rewritten as

$$\sum_{p=1}^{\infty} \frac{J_m(p\delta)J_n(p\delta)}{p} = \sum_{p=1}^{\infty} \frac{J_m(p\delta)J_n(p\delta)}{p\delta}\delta.$$

Let $\delta \to \Delta x$, a differential form of $x$, then $p\delta = x_i$. The above summation then becomes

$$\lim_{k\to\infty}\sum_{i=1}^{k}\frac{J_m(x_i)J_n(x_i)}{x_i}\Delta x=\int_0^{\infty}\frac{J_m(x)J_n(x)}{x}\mathrm{d}x. \tag{36}$$

Using the Weber-Schafheitlin formula (MacLachlan, 1934), the integral in (36) can be written as

$$\frac{\Gamma\left[\frac{1}{2}(m+n)\right]}{2\Gamma(n+1)\Gamma\left[\frac{1}{2}(m-n+2)\right]}\times F\left[\frac{1}{2}(n-m),\quad \frac{1}{2}(n+m),\quad (n+1),\quad 1\right] \tag{37}$$

where $\Gamma$ is the Gamma function and $F$ is the hypergeometric function

$$F(\alpha,\beta,\gamma,z)=\left\{1+\frac{\alpha\beta z}{1!\gamma}+\frac{\alpha(\alpha+1)\beta(\beta+1)z^2}{2!\gamma(\gamma+1)}+\cdots\right\}. \tag{38}$$

Note that $F$ is one of the solutions of Gauss's equation

$$z(1-z)\frac{\mathrm{d}^2y}{\mathrm{d}z^2}+\{\gamma-z(\alpha+\beta+1)\}\frac{\mathrm{d}y}{\mathrm{d}z}-\alpha\beta y=0,\quad \text{and that}$$

$$F(\alpha,\beta,\gamma,1)=\frac{\Gamma(\gamma)\Gamma(\gamma-\alpha-\beta)}{\Gamma(\gamma-\alpha)\Gamma(\gamma-\beta)}. \tag{39}$$

Using eqns (36), (37) and (39), we find that if the crack length is small ($\delta\leqslant 0.01$ in our program),

$$\sum_{p=1}^{\infty}\frac{J_m(p\delta)J_n(p\delta)}{p}=\frac{\delta_{mn}}{2n}. \tag{40}$$

For the dynamic case, where the frequencies of the incident wave are such that $k_1a$ is less than 0.1 in our program, an iterative scheme needs to be employed. Because the $I_n$ terms in (31), (32) and (33) contain, in the integral in the last equation of (34), the $K/k_1$ variable, eqn (35) cannot be solved explicitly. Hence an iterative method is used starting with the static value of $K/k_1$. Substituting the static value of $K/k_1$ in the last equation of (34), initial values of $I_n$ are obtained. Then using these initial values for (35), we can get the initial value of $K/k_1$. Following the same procedures, converging values of $K/k_1$ is then obtained.

## 6. NUMERICAL RESULTS

In our program, we test the applicability of a composite material in which the fibers have stiffer shear modulus and lighter weight than the matrix does ($\mu_1=1.28\,\mathrm{e}^{10}$ Pa, $\mu_2=8.08\,\mathrm{e}^{10}$, $\rho_1=801$ Kg/m$^3$, $\rho_2=234.7$ Kg/m$^3$). The two extreme debonded situations are when there is no crack ($\delta=0$) and when the fibers are totally debonded from the matrix ($\delta=\pi$, regarded as the case when the space occupied by the fibers is void). For these two extreme cases, the resultant computational shear moduli from our program coincide with those obtained by Hashin and Rosen (1964). Obviously, these two extreme cases render

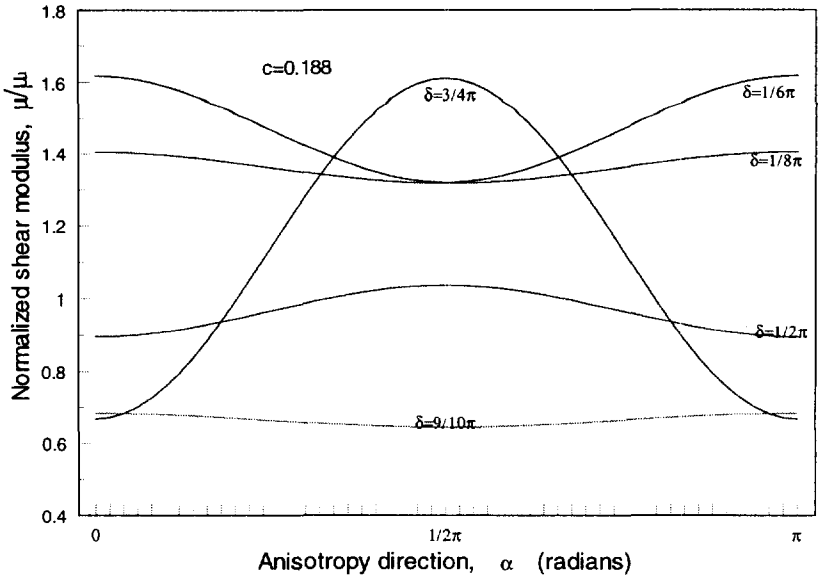


Fig. 3. Using normalized shear modulus as a function of anisotropic directions to demonstrate the transverse anisotropy properties for various cases of half crack length at 0.188 fiber vol. fraction.

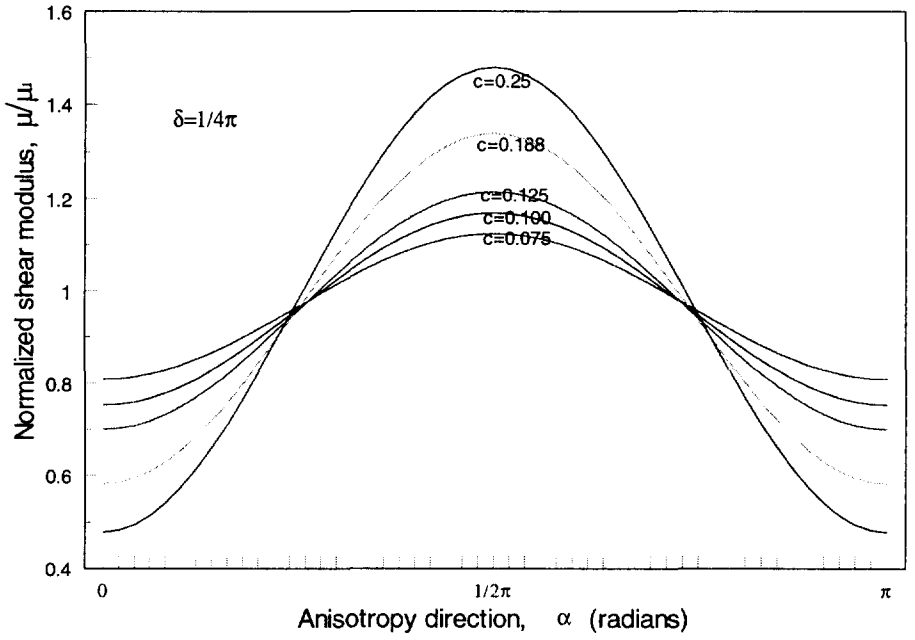


Fig. 4. Using normalized shear modulus as a function of anisotropic directions to demonstrate the transverse anisotropy properties for various cases of fiber vol. fraction at $1/4\pi$ half crack length.

the composite system as transversely isotropic. When the fibers are partially bonded, the composite system becomes transversely anisotropic as can be seen in Figs 3, 4, 5 and 6.

The computational quantities obtained using eqn (35) are normalized wave numbers and are generally complex. In the static case, the magnitude of the imaginary part of $\mu/\mu_1$ (obtained from the normalized wave number $K/k_1$) is extremely small compared to that of the real part. This granted us the justification that, for the static case, the shear modulus is a real number and it corresponds to the elasticity of the composite system. While for the dynamic case, the magnitude of the imaginary part of $\mu/\mu_1$ is significant compared to that of the real part and it corresponds to the dissipative part of the composite system. Only the

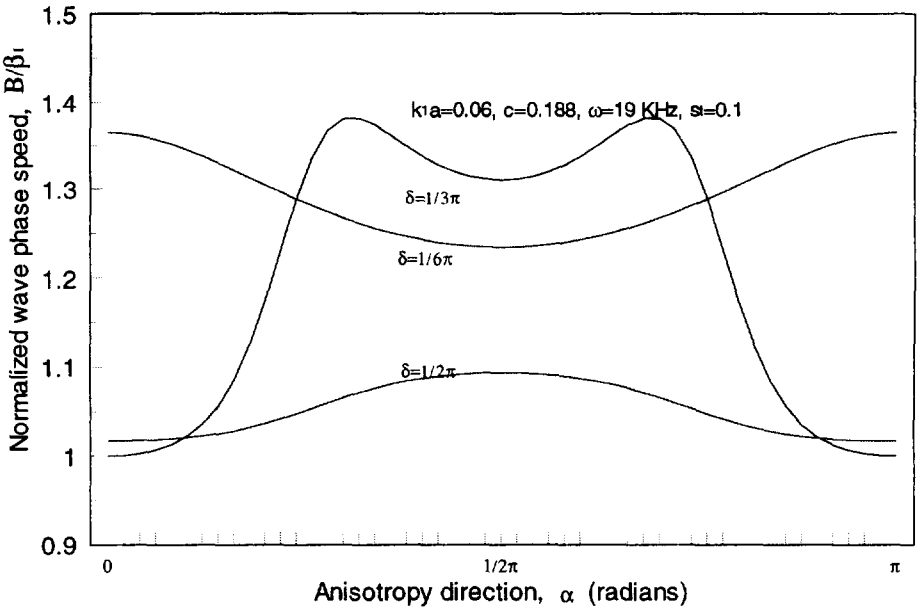


Fig. 5. Using normalized shear wave phase speed as a function of anisotropic directions to demonstrate the transverse anisotropy properties for various cases of half crack length at 0.188 fiber vol. fraction.

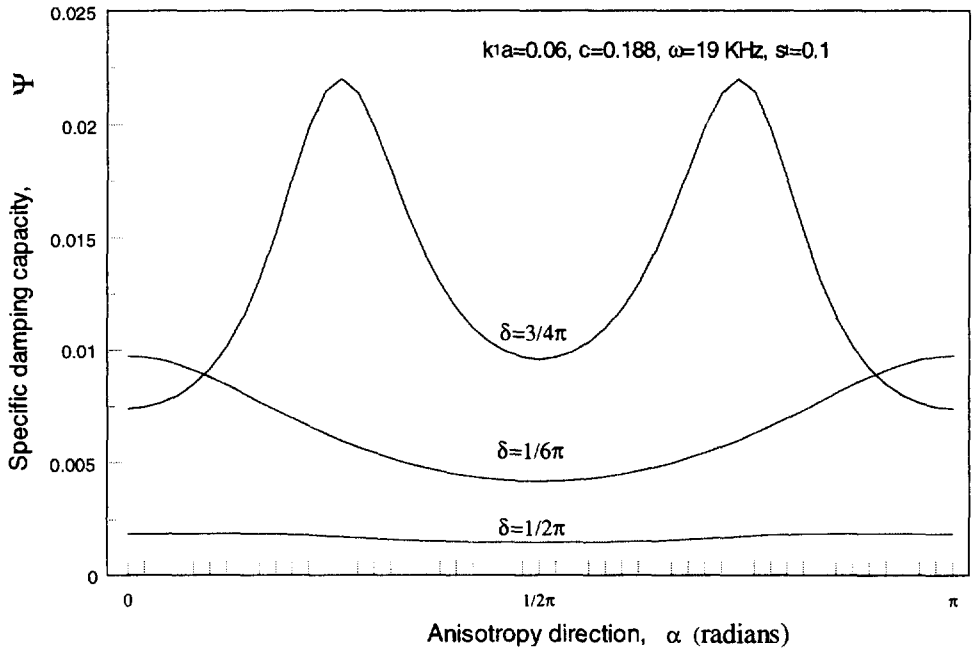


Fig. 6. Using specific damping capacity as a function of anisotropic directions to demonstrate the transverse anisotropy properties for various cases of half crack length at 0.188 fiber vol. fraction.

fact that, for some ranges of half crack length, the calculated shear moduli, the shear wave phase speeds and specific damping capacities are negative numbers or extremely high conflict with the physics of the composite system (Figs 7, 8, 9 and 10). These 'jumps' occur in some particular ranges of half crack length for a variety of cases. As it turns out, the increase of the number of summation terms in our program does not change the resultant magnitude of interest associated with the jumps (in other words, the converging is achieved).

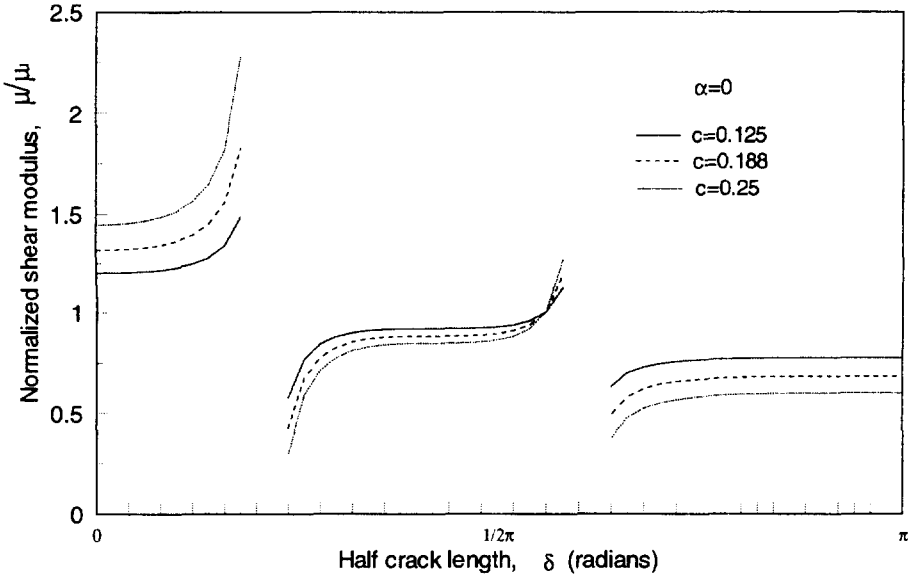


Fig. 7. Normalized shear modulus as a function of half crack lengths for various cases of fiber vol. fraction at zero anisotropic direction. Note the 'decreasing steps' fashion as the half crack length increases. Also, the jumps occur near $11/50\pi$, $31/50\pi$.

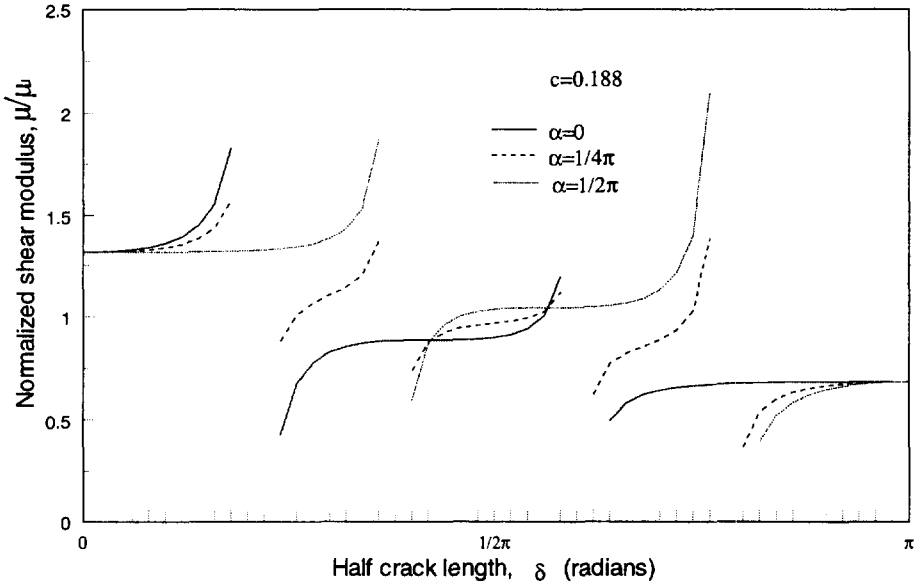


Fig. 8. Normalized shear modulus as a function of half crack lengths for various cases of anisotropic direction at 0.188 fiber vol. fraction. Note the 'decreasing steps' fashion as the half crack length increases. Also, for $\alpha = 1/2\pi$, jumps occur $19.50\pi$, $39/50\pi$. For $\alpha = 1/4p$, jumps occur near $11/50\pi$, $19/50\pi$, $31/50\pi$, $39/50\pi$. For $\alpha = 0$, jumps occur near $11/50\pi$, $31/50\pi$.

Therefore the mathematical facts of these 'anomalies' are confirmed and those jumps are finite.

An interesting phenomenon of the transverse anisotropy of the composite system is that it is less pronounced near three ranges of the half crack length. Two of them are, expectantly, near $\delta = 0$ and $\delta = \pi$. The other one is near, surprisingly, $\delta = \pi/2$ (Fig. 3). Another factor that affects the transverse anisotropy of the composite system is that of the fiber volume fraction. As expected, the less the fiber volume concentration, the less anisotropic is the system. Observing Figs 4 and 7, if the fiber volume fraction is small, then the

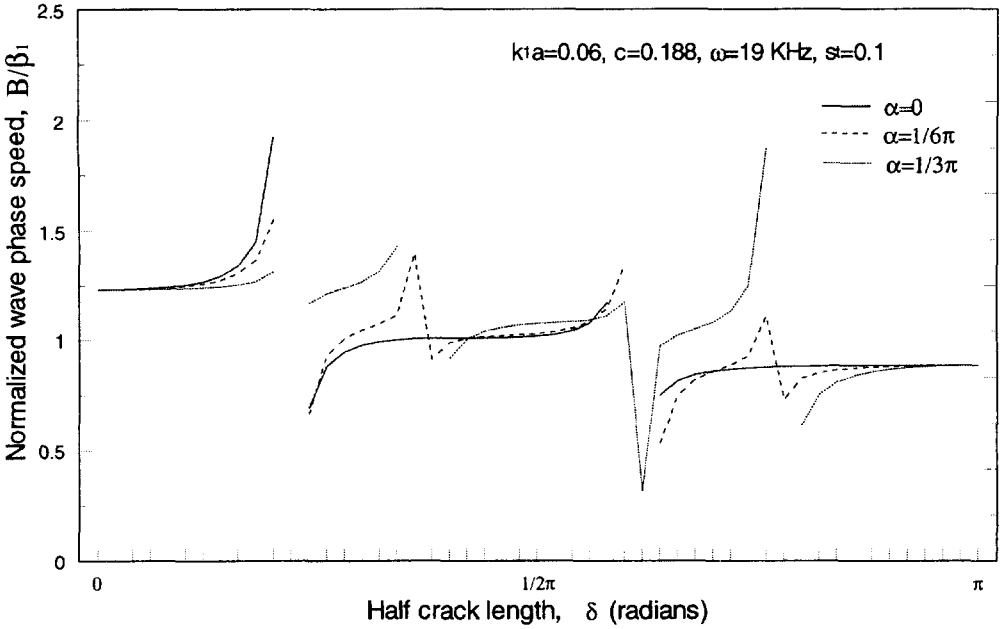


Fig. 9. Normalized shear wave phase speed as a function of half crack lengths for various cases of anisotropic direction at 0.188 fiber vol. fraction. The 'decreasing steps' fashion has the same properties as those of the shear modulus. Note that for $\alpha = 1/3\pi$, jumps occur near $11/50\pi$, $19/50\pi$, $39/50\pi$. For $\alpha = 1/6\pi$, jumps occur near $11/50\pi$, $31/50\pi$. For $\alpha = 0$, jumps occur near $11/50\pi$, $31/50\pi$.

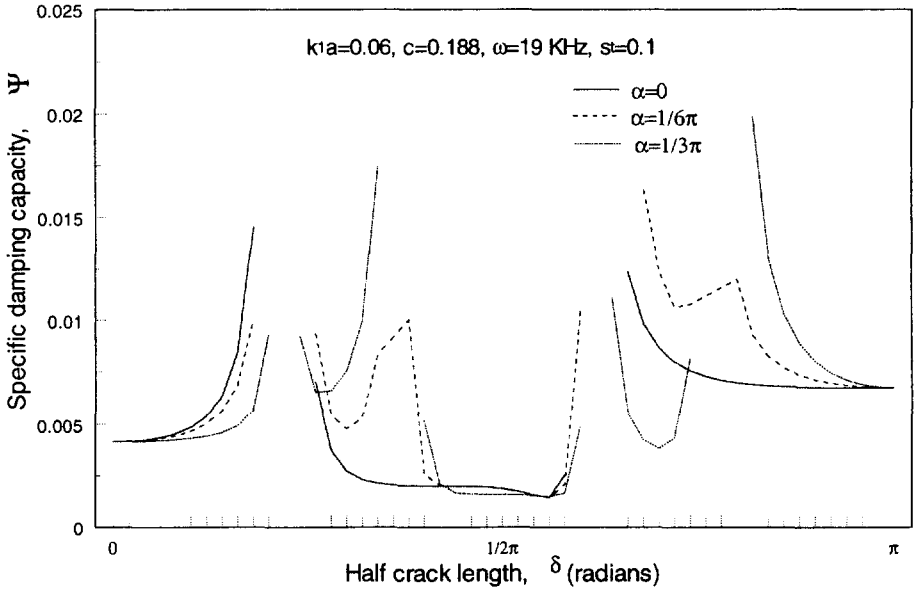


Fig. 10. Specific damping capacity as a function of half crack lengths for various cases of anisotropic direction at 0.188 fiber vol. fraction. Note that the least lossy is near the mid-ranges of half crack length. Also, for $\alpha = 1/3\pi$, jumps occur near $11/50\pi$, $19.50\pi$, $31/50\pi$, $39/50\pi$. For $\alpha = 1/6\pi$, jumps occur near $11/50\pi$, $31/50\pi$. For $\alpha = 0$, jumps occur near $11/50\pi$, $31/50\pi$.

quantity of $\mu/\mu_1$ will be near 1 and the function line will tend to be 'flat' and near 1. While for higher quantities of '$c$', the $\mu/\mu_1$ curve will be increasingly less 'flat' and the value of it farther from 1.

Observing Figs 7, 8 and 9, the shear moduli and the wave speeds are decreasing in a step-by-step fashion. For each step, the function line is generally leveled before it reaches the jump area. The same feature occurs for the damping capacity in Fig. 10, except that the minimum quantity of the damping capacity occurs at the middle step where $1/2\pi$ half crack

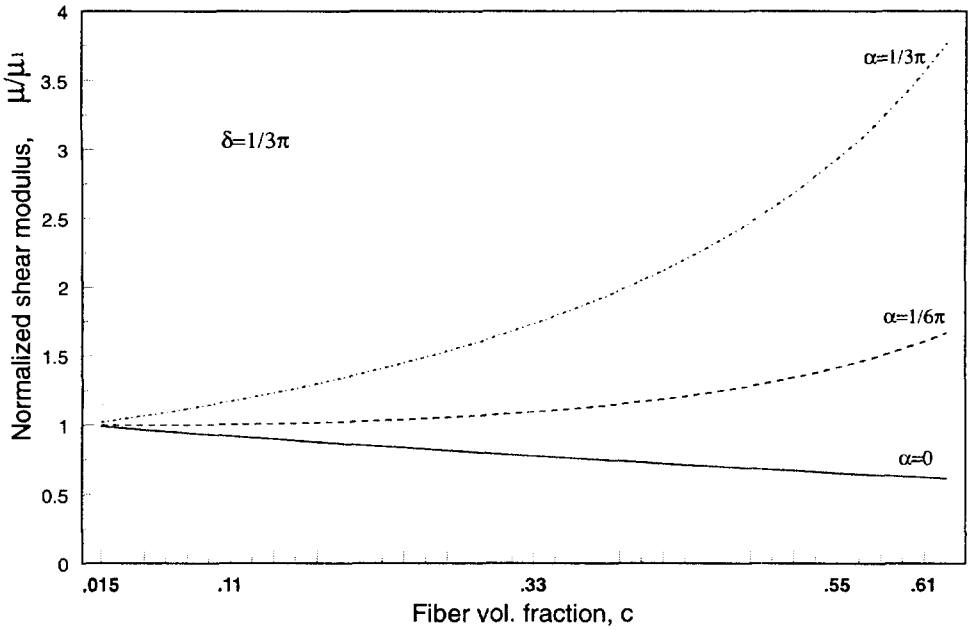


Fig. 11. Normalized shear modulus as a function of fiber vol. fraction for various cases of anisotropic directions at $1/3\pi$ half crack length. Note that a 'critical pair' exists when $\delta = 1/3\pi$ and when a specific anisotropic direction is between '0' and '$1/6\pi$'.

length locates. In Fig. 7, the jumps, given a fixed anisotropic direction $\alpha = 0$, occur at the same ranges of half crack length for various fiber volume fraction. Figures 8, 9 and 10 show that the jumps locations are generally different for different anisotropic directions. Interestingly, the numerical jump regions always occur near one or more of four half crack length regions, i.e., $11/50\pi$, $19/50\pi$, $31/50\pi$ and $39/50\pi$.

The influence of fiber volume fraction ('$c$') on the normalized shear modulus, as can be seen from Figs 4 and 7, has different trends for different ranges of half crack length and anisotropic direction. Roughly, there exist 'critical pairs' of $\delta$ and $\alpha$ that the quantity of $\mu/\mu_1$ stays approximately constant for any '$c$' (as long as '$c$' is low—$c \leqslant 0.25$ is sufficient for our case). More specifically, in Fig. 7, a normalized shear modulus of approximate magnitude of 1 exists when $\alpha = 0$ and $\delta$ is near $28/50\pi$. Two other critical pairs of $\alpha$ and $\delta$ exist in the 'jump area' where different constant quantities of $\mu/\mu_1$ exist. This means that the shear stiffness of a composite system, with zero anisotropic direction and $\delta \cong 28/50\pi$, stays constant for any fiber volume fraction if $c \leqslant 0.25$. Similarly in Fig. 4, two critical pairs of $\delta$ and $\alpha$ ($\delta = 1/4\pi$, $\alpha$ near $12/50\pi$ or $38/50\pi$) render a normalized shear modulus of approximately 0.94 for $0.075 \leqslant c \leqslant 0.25$. This 'critical pair' phenomenon can also be seen in Figs 11 and 12. In Fig. 11, the influence of '$c$' on $\mu/\mu_1$ is in an inverse fashion for $\alpha = 0$ and not for $\alpha = 1/6\pi$. Therefore we predict that, given a known half crack length of $1/3\pi$, there exists an $\alpha$ between 0 and $1/6\pi$ where the magnitude of the fiber volume fraction (for $c \leqslant 0.25$, at least) does not have any influence on the stiffness of the composite. Similarly, in Fig. 12, there exists a $\delta$ between $1/2\pi$ and $1/3\pi$ where the change of '$c$' (for $c \leqslant 0.25$) does not affect the shear stiffness of the composite.

The influences of anisotropic direction ($\alpha$) and half crack length ($\delta$) on the stiffness of the composite can be observed in Figs 11 and 12, respectively. Figure 11 shows that the composite system is stiffer for larger anisotropic direction. And this is generally the trend in Fig. 8 except on both end sides of half crack length. Figure 12 shows that, at $\alpha = 1/4\pi$, the lesser the half crack length the stiffer the composite is. This generally reflects the fact that the stiffness of the composite decreases as the half crack length increases (Figs 7 and 8).

For dynamic mechanical properties, Fig. 13 shows that the higher the fiber volume fraction (we fix the quantity of the fiber radius and vary the number of fibers per unit cross

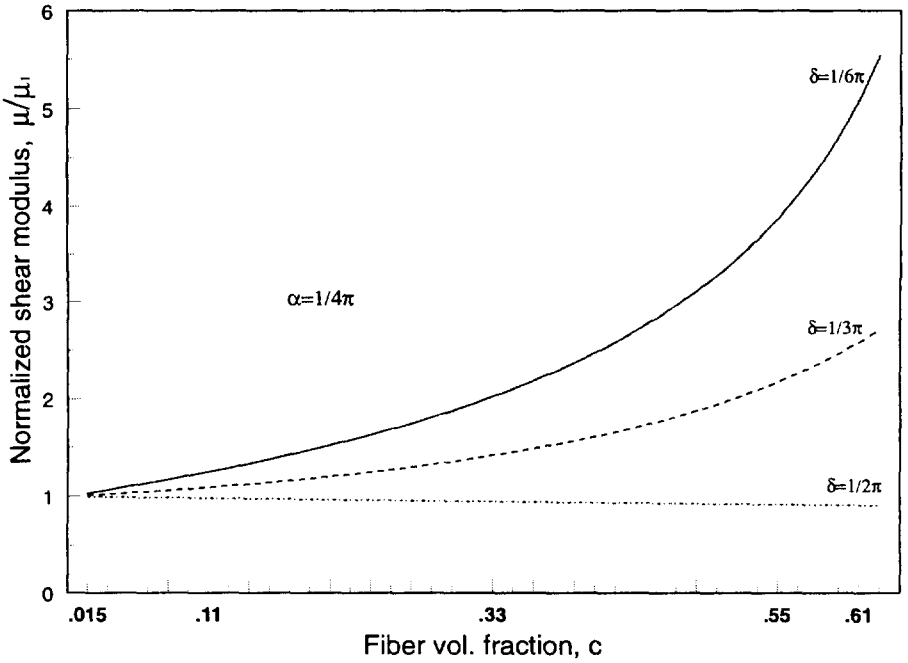


Fig. 12. Normalized shear modulus as a function of fiber vol. fraction for various cases of half crack lengths at $1/4\pi$ anisotropic direction. Note that a 'critical pair' exists when $\alpha = 1/4\pi$ and when a specific half crack length $d$ is between '$1/3\pi$' and '$1/2\pi$'.

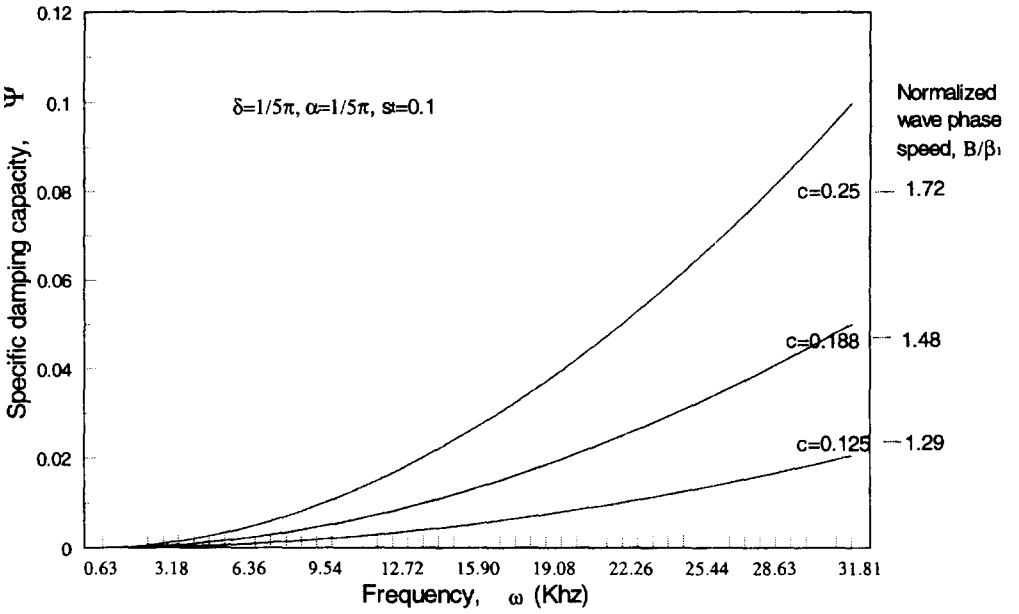


Fig. 13. Specific damping capacity as a function of wave frequencies for various cases of fiber vol. fraction at $1/5\pi$ half crack length and $1/5\pi$ anisotropic direction. Note that the normalized shear wave phase speed does not change for the low frequency ranges.

sectional area) the more damping of the composite and the faster the shear wave phase speed. Figure 14 shows that, given a fixed half crack length, the shear wave phase speeds are roughly the same for various anisotropic direction. And the change of damping capacity as a function of $\alpha$ is an inverse relationship when $\delta = 1/8\pi$. In Fig. 15, the change of the wave speeds, given a fixed anisotropic direction of $\alpha = 0$, also show the 'decreasing step' fashion as a function of the half crack length. Also in Fig. 15, the damping capacity has the lowest quantity in the middle section of $\delta$ (where $\delta$ is near $1/2\pi$)—this reflects the same

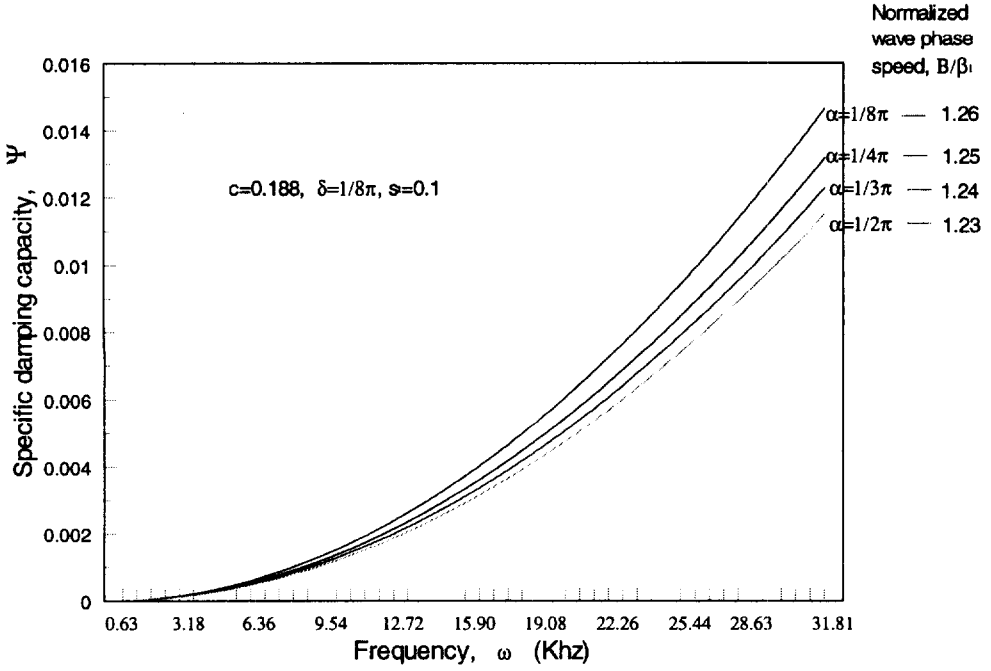


Fig. 14. Specific damping capacity as a function of wave frequencies for various cases of anisotropic directions at $1/8\pi$ half crack length and 0.188 fiber vol. fraction. Note that the normalized shear wave phase speed does not change for the low frequency ranges. Also, the change of anisotropic direction does not influence the shear wave phase speed.

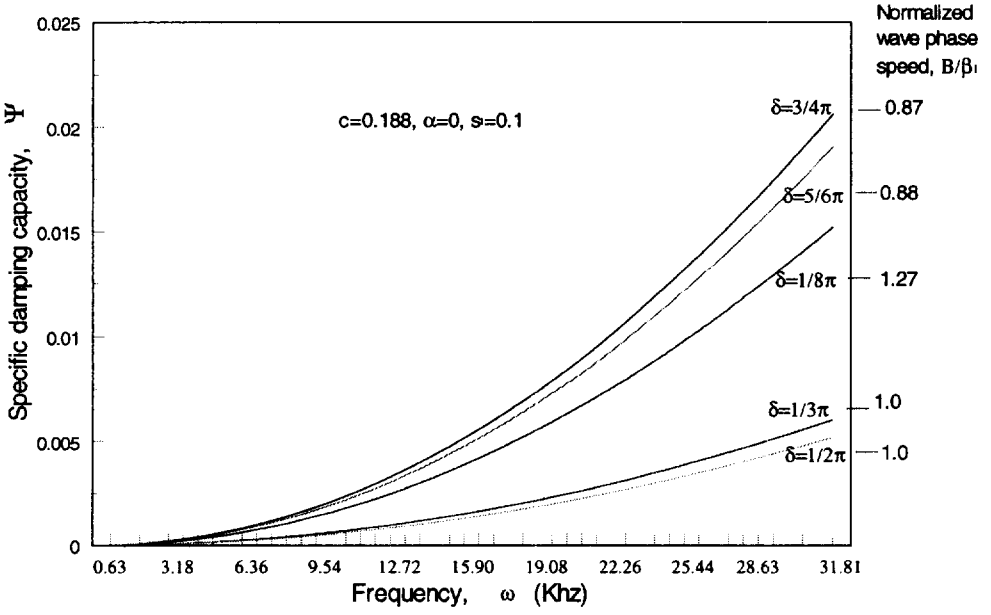


Fig. 15. Specific damping capacity as a function of wave frequencies for various cases of half crack lengths at zero anisotropic direction and 0.188 fiber vol. fraction. Note that the normalized shear wave phase speed does not change for the low frequency ranges. Also, the least lossy is near the mid-ranges of half crack length and normalized shear wave speed is in a 'decreasing steps' fashion as the half crack length increases.

trends as in Fig. 10. Finally, from Figs 13, 14 and 15, the influence of frequencies (low frequencies such that $k_1 a < 0.1$) on the wave speeds is non-existent, while it is significant on the damping capacity. Therefore the composite system is non-dispersive and highly viscoelastic in the low frequency range.

## 7. CONCLUDING REMARKS

The material modeling of the composite system with interfacial cracks has been carried out using straightforward yet rigorous mathematical treatments. An attempt is made to characterize the overall effective mechanical properties of the composite system. For our model, the computational results (normalized shear moduli) of the two extreme bonding situations ($\delta = 0$ and $\delta = \pi$) are exactly the same as those obtained by the classical formula (Hashin and Rosen, 1964). Our model demonstrates the transversely anisotropic properties of the composite system and it confirms the transverse isotropy at the two extreme bonding situations and at a low fiber volume fraction. In addition, it predicts the transverse isotropy of the material system when the half crack length is near $1/2\pi$. Further, the stiffness of the composite (shear modulus $\mu$), as we increase the half crack length, is decreasing in a step-by-step fashion from the state of perfect bonding ($\delta = 0$) to the state of totally debonding ($\delta = \pi$). For each individual step, the quantity of $\mu$ is generally leveled until it reaches the jump region. Therefore, in general, the model predicts the weakening of the shear stiffness of the composite as the half crack length grows in spite of the fact that there exists the 'jump anomalies'. The wave speeds exhibit the same general trend as the shear moduli do. And the damping capacity, generally, has the lowest quantity in the middle section of half crack length ranges (near $\delta = 1/2\pi$). In addition, the total debonding case has a higher quantity of damping capacity than the perfect bonding one. Finally the model predicts the composite system is non-dispersive in the low frequencies ranges. And the change of frequency has tangible effects on the change of specific damping capacity.

In retrospect, our model does not claim to be quantitatively precise to predict the behavior of the composite system, as the numerical jumps of the normalized shear moduli clearly show. But more importantly the general trends of the calculated strength and the dynamic properties are what we can take into account in designing or inspecting a composite material system.

*Acknowledgments*—The authors wish to express thanks for support provided by NSF Science and Technology Center for High Performance Polymeric Adhesives and Composite, contract DMR9120004. Also, this work was partially supported by the National Center for Supercomputing Applications under grant number DMR950003N and utilized the computer system Silicon Graphics Power Challenge Array at the National Center for Supercomputing Applications, University of Illinois at Urbana-Champaign.

## REFERENCES

Aboudi, J. (1988) Wave propagation in damaged composite materials. *International Journal of Solids and Structures* **24,** 117–138.

Angel, Y. C. (1988) On the reduction of elastodynamic crack problems to singular integral equations. *International Journal of Engineering Science* **26,** 757–764.

Angel, Y. C. and Koba, Y. K. (1993) Propagation of antiplane waves in a multi-cracked solid. *AMD*, **158,** *Anisotropy and Inhomogeneity in Elasticity and Plasticity*, *ASME* 51–57.

Arfken, G. (1970) *Mathematical Methods for Physicists*, pp. 628. 2nd ed., Academic Press.

Bose, S. K. and Mal, A. K. (1973) Longitudinal shear waves in a fiber-reinforced composite. *International Journal of Solids and Structures* **9,** 1075–1085.

Bose, S. K. and Mal, A. K. (1974) Elastic waves in a fiber-reinforced composite. *Journal of the Mechanics and Physics of Solids* **22,** 217–229.

Coussy, O. (1984) Scattering of elastic waves by an inclusion with an interface crack. *Wave Motion* **6,** 223–236.

Coussy, O. (1986a) Scattering of SH-waves by a rigid elliptic fiber partially debonded from its surrounding matrix. *Mechanics Research Communications* **13,** 39–45.

Coussy, O. (1986b) The influence of interface cracks on wave motion in fiber reinforced elastic solids. *Journal of Theoretical and Applied Mechanics* **5,** 803–823.

Datta, S. K., Ledbetter, H. M. and Kriz, R. D. (1984) Calculated elastic constants of composites containing anisotropic fibers. *International Journal of Solids and Structures* **20,** 429–438.

Hashin, Z. and Rosen, B. W. (1964) The elastic module of fiber-reinforced materials. *Journal of Applied Mechanics* **31,** 223.

Krenk, S. and Schmidt, H. (1982) Elastic wave scattering by a circular crack. *Philosophical Transactions of the Royal Society of London* **A308,** 167–198.

Mal, A. K., Yin, C.-C. and Bar-Cohen, Y. (1991) Ultrasonic nondestructive evaluation of cracked composite laminates. *Composites Engineering* **1,** 85–101.

McLachlan, N. W. (1934) *Bessel Functions for Engineers*. p. 56, 59, 91. Oxford University Press, Oxford, U.K.

Neerhoff, F. L. (1979) Diffraction of love waves by a stress-free crack of finite width in the plane interface of a layered composite. *Applied Scientific Research* **35,** 265–315.

Waterman, P. C. and Truell, R. (1961) Multiple scattering of waves. *Journal of Mathematical Physics* **2,** 512–537.

Yang, R.-B. and Mal, A. K. (1994) Multiple scattering of elastic waves in a fiber-reinforced composite. *Journal of the Mechanics and Physics of Solids* **42**(12), 1945–1968.
Yang, Y. and Norris, A. N. (1991) Shear wave scattering from a debonded fiber. *Journal of the Mechanics and Physics of Solids* **39,** 273–294.

## APPENDIX A

The generating function of the Chebyshev polynomial (Arfken, 1970) is defined as

$$T_n(x)+iV_n(x) = [x+i(1-x^2)^{1/2}]^n, \quad |x| \leqslant 1 \tag{A1}$$

where

$$\begin{aligned} T_n(x) &= x^n - \binom{n}{2}x^{n-2}(1-x^2)+\binom{n}{4}x^{n-4}(1-x^2)^2-\cdots \\ V_{n+1}(x) &= \sqrt{1-x^2}\,U_n(x) \\ U_n(x) &= \left[\binom{n+1}{1}x^n-\binom{n+1}{3}x^{n-2}(1-x^2)+\binom{n+1}{5}x^{n-4}(1-x^2)^2-\cdots\right] \end{aligned} \tag{A2}$$

$T_n(x)$ is the Chebyshev function of type I and $U_n(x)$ is the Chebyshev function of type II. Rewrite $V_n(x)$ as

$$V_n(x) = \sqrt{1-x^2}\left[\binom{n}{1}x^{n-1}-\binom{n}{3}x^{n-3}(1-x^2)+\binom{n}{5}x^{n-5}(1-x^2)^2-\cdots\right], \quad n = 1, 2, 3\ldots \tag{A3}$$

Note that for $x \to \pm 1$, $V_n(x) \to O(\sqrt{1-(1-\varepsilon)^2})$ i.e., $V_n(x) \to O(\varepsilon^{1/2})$ as $x$ approaches $\pm 1$. Let $x = \cos\theta$ in eqn (A1), then

$$\begin{aligned} T_n(x)+iV_n(x) &= e^{in\theta}. \quad \text{Therefore} \\ T_n(x) &= \cos n\theta = \cos(n\cos^{-1}x) \\ V_n(x) &= \sin n\theta = \sin(n\cos^{-1}x). \end{aligned} \tag{A4}$$

Furthermore, let $\theta = \pi/2-\alpha$. Thus $x = \cos\theta = \cos(\pi/2-\alpha) = \sin\alpha$. Accordingly

$$V_n(x) = \sin n\theta = \sin n(\pi/2-\alpha) = \sin(n\pi/2-n\sin^{-1}x) \quad n = 1, 2, 3\ldots \tag{A5}$$

The following formulae are used to perform integration involving Chebychev function:

$$\begin{aligned} \int_0^{2\pi} e^{iz\cos\theta}\cos n\theta\,\mathrm{d}\theta &= 2\pi i^n J_n(z) \\ \int_0^{2\pi} e^{iz\cos\theta}\sin n\theta\,\mathrm{d}\theta &= 0 \\ \int_0^{2\pi} e^{iz\cos\theta}e^{in\theta}\,\mathrm{d}\theta &= 2\pi i^n J_n(z) \\ J_{n-1}(x)+J_{n+1}(x) &= \frac{2n}{x}J_n(x) \end{aligned} \tag{A6}$$

The integration of Chebychev function is performed as the following

$$\begin{aligned} \phi_n(\theta_i) = \frac{1}{n}V_n\left(\frac{\theta_i-\varphi_i}{\delta_i}\right) = \frac{1}{n}\sin\left(\frac{n\pi}{2}-n\sin^{-1}\frac{\theta_i-\varphi_i}{\delta_i}\right), \quad n = 1, 2, 3\ldots \int_{-\delta_i+\varphi_i}^{\delta_i+\varphi_i}\phi_n(\theta_i)\,e^{-ip(\theta_j-\theta_0)}\,\mathrm{d}\theta_j \\ = e^{ip\theta_0}\frac{1}{n}\int_{-\delta_i+\varphi_i}^{\delta_i+\varphi_i}\sin\left(n\pi/2-n\sin^{-1}\frac{\theta_j-\varphi_i}{\delta_i}\right)e^{-ip\theta_j}\,\mathrm{d}\theta_j, \end{aligned} \tag{A7}$$

let $\sin^{-1}\theta_i-\varphi_i/\delta_i=\tau'$, then $\sin\tau'=\theta_i-\varphi_i/\delta_i$, and $\mathrm{d}\theta_i=\delta_i\cos\tau'\,\mathrm{d}\tau'$. In addition let $\tau'=\tau-\pi/2$ then eqn (A7) becomes

$$e^{ip\theta_0}\frac{1}{n}\int_{-\pi/2}^{\pi/2}\sin(n\pi/2-n\tau')\,e^{-ip(\varphi_i-\delta_i\sin\tau')}\delta_i\cos\tau'\,\mathrm{d}\tau'$$

$$=(-1)^{n+1}e^{ip(\theta_0-\varphi_i)}\frac{\delta_i}{n}\frac{1}{4}\int_{-\pi}^{\pi}e^{ip\delta_i\cos\tau}[\cos(n-1)\tau-\cos(n+1)\tau]\,\mathrm{d}\tau. \quad \text{(A8)}$$

Summarily, the integration of Chebychev function is

$$\int_{-\delta_i+\varphi_i}^{\delta_i+\varphi_i}\phi_n(\theta_i)\,e^{-ip(\theta_i-\theta_0}\,\mathrm{d}\theta_i=\begin{cases}\dfrac{(-1)^{n+1}\pi\delta_i}{2n}\delta_{1n}, & p=0\\ e^{ip(\theta_0-\varphi_i)}\dfrac{\pi}{p}i^{n+1}J_n(-p\delta_i), & p\neq 0\end{cases},\quad n=1,2,3\ldots \quad \text{(A9)}$$

## APPENDIX B

$$a_{11}=\begin{bmatrix} a_{11,mm} & & & & a_{11,m1}\\ & \ddots & & & \vdots\\ & & \ddots & & \vdots\\ & & & a_{11,22} & a_{11,21}\\ a_{11,1m} & \cdots & \cdots & a_{11,12} & a_{11,11}\end{bmatrix} \quad \text{(B1)}$$

$$a_{11,rm}=\begin{cases}\dfrac{z}{\left(\dfrac{\mu_2}{\mu_1}-1\right)}\dfrac{k_1}{k_2}\displaystyle\sum_{n=1}^{\infty}\sum_{p=1}^{\infty}q_{np,i}J_n(\delta_i)[e^{-i\alpha}+e^{i\alpha}(-1)^n](X_{p1}i^{n-3}+Y_{p1}i^{n+1})\\ \qquad +2(1+cu_1)+\pi icu_1(I_0-I_2), \quad r=m=1\\ \dfrac{z}{(m-1)!\left(\dfrac{\mu_2}{\mu_1}-1\right)}\dfrac{k_1}{k_2}2^{m-1}\displaystyle\sum_{n=1}^{\infty}\sum_{p=1}^{\infty}q_{np,i}J_n(m\delta_i)[e^{-im\alpha}+e^{im\alpha}(-1)^n]\\ \qquad \times(X_{pm}i^{n+2m-1}+Y_{pm}i^{n+1})+2, \quad r=m\neq 1\\ \dfrac{z}{(m-1)!\left(\dfrac{\mu_2}{\mu_1}-1\right)}\dfrac{k_1}{k_2}2^{m-1}\displaystyle\sum_{n=1}^{\infty}\sum_{p=1}^{\infty}q_{np,i}J_n(m\delta_i)[e^{-im\alpha}+e^{im\alpha}(-1)^n]\\ \qquad \times(X_{p1}i^{n-r-m-1}+Y_{p1}i^{n+r-m+1}), \quad r\neq m\end{cases} \quad \text{(B2)}$$

$$a_{12}=\begin{bmatrix} a_{12,m1} & & & & a_{12,mm} & a_{12,m2} & & & a_{12,mm}\\ \vdots & & & \iddots & & \vdots & & \iddots & \\ \vdots & & \iddots & & & \vdots & \iddots & & \\ a_{12,21} & a_{12,22} & & & & a_{12,22} & & & \\ a_{12,11} & a_{12,12} & \cdots & \cdots & a_{12,1m} & a_{12,12} & \cdots & \cdots & a_{12,1m}\end{bmatrix}=\begin{bmatrix} a_{12,m1} & & & & a_{12,mm}\\ \vdots & & & \iddots & \\ \vdots & & \iddots & & \\ a_{12,21} & a_{12,22} & & & \\ a_{12,11} & a_{12,12} & \cdots & \cdots & a_{12,1m}\end{bmatrix}+\begin{bmatrix} a_{12,m2} & & & a_{12,mm}\\ \vdots & & \iddots & \\ \vdots & \iddots & & \\ a_{12,22} & & & \\ a_{12,12} & \cdots & \cdots & a_{12,1m}\end{bmatrix}=a_{12}+a'_{12} \quad \text{(B3)}$$

$$a_{12,m}=\begin{cases}\dfrac{z}{\left(\dfrac{\mu_2}{\mu_1}-1\right)}\dfrac{k_1}{k_2}\displaystyle\sum_{n=1}^{\infty}\sum_{p=1}^{\infty}q_{np,i}Y_{p1}i^{n-1}J_n(\delta_i)[e^{-i\alpha}+e^{i\alpha}(-1)^n]-(1+cu_1)+\frac{\pi}{2}icu_1(I_2-I_0), \quad r=m=1\\ \dfrac{z}{(m-1)!\left(\dfrac{\mu_2}{\mu_1}-1\right)}\dfrac{k_1}{k_2}2^{m-1}\displaystyle\sum_{n=1}^{\infty}\sum_{p=1}^{\infty}q_{np,i}Y_{pm}i^{n-1}J_n(m\delta_i)[e^{-im\alpha}+e^{im\alpha}(-1)^n]-1, \quad r=m\neq 1\\ \dfrac{z}{(m-1)!\left(\dfrac{\mu_2}{\mu_1}-1\right)}\dfrac{k_1}{k_2}2^{m-1}\displaystyle\sum_{n=1}^{\infty}\sum_{p=1}^{\infty}q_{np,i}Y_{pr}i^{n+r-m-1}J_n(m\delta_i)[e^{-im\alpha}+e^{im\alpha}(-1)^n], \quad r\neq m\end{cases} \quad \text{(B4)}$$

$$a_{21}=\begin{bmatrix} a_{21,1m} & \cdots & \cdots & a_{21,12} & a_{21,11} \\ & & & a_{21,22} & a_{21,21} \\ & & \iddots & \vdots & \\ & \iddots & & \vdots & \\ a_{21,mm} & & & a_{21,m1} & \end{bmatrix}, \quad a'_{21}=\begin{bmatrix} a_{21,2m} & \cdots & \cdots & a_{21,22} & a_{21,21} \\ & & \iddots & & \vdots \\ & \iddots & & & \vdots \\ a_{21,mm} & & & & a_{21,m1} \end{bmatrix} \tag{B5}$$

$$a_{21,rm}=\begin{cases} \dfrac{ze^{i\alpha}}{\left(\dfrac{\mu_2}{\mu_1}-1\right)}\dfrac{k_1}{k_2}\displaystyle\sum_{n=1}^{\infty}\sum_{p=1}^{\alpha} q_{np,i}J_n(\delta_i)(-1)^n(X_{p1}i^{n-1}+Y_{p1}i^{n-1}) \\ \quad -(1+cu_1)+\dfrac{\pi}{2}icu_1(I_2-I_0), \quad r=m=1 \\ \dfrac{ze^{im\alpha}}{(m-1)!\left(\dfrac{\mu_2}{\mu_1}-1\right)}\dfrac{k_1}{k_2}2^{m-1}\displaystyle\sum_{n=1}^{\infty}\sum_{p=1}^{\alpha} q_{np,i}J_n(m\delta_i)(-1)^n \\ \quad \times(X_{pm}i^{n-2m+1}+Y_{pm}i^{n-1})-1, \quad r=m\neq 1 \\ \dfrac{ze^{im\alpha}}{(m-1)!\left(\dfrac{\mu_2}{\mu_1}-1\right)}\dfrac{k_1}{k_2}2^{m-1}\displaystyle\sum_{n=1}^{\infty}\sum_{p=1}^{\alpha} q_{np,i}J_n(m\delta_i)(-1)^n \\ \quad \times(X_{pr}i^{n-r-m+1}+Y_{pr}i^{n-r-m-1}), \quad r\neq m \end{cases} \tag{B6}$$

$$a_{22}=\begin{bmatrix} a_{22,11} & a_{22,12} & \cdots & \cdots & a_{22,1m} \\ a_{22,21} & a_{22,22} & & & \\ \vdots & & \ddots & & \\ \vdots & & & \ddots & \\ a_{22,m1} & & & & a_{22,mm} \end{bmatrix}, \quad a'_{22}=\begin{bmatrix} a_{22,22} & \cdots & \cdots & a_{22,2m} \\ \vdots & \ddots & & \\ \vdots & & \ddots & \\ a_{22,m2} & & & a_{22,mm} \end{bmatrix} \tag{B7}$$

$$a_{22,rm}=\begin{cases} \dfrac{ze^{i\alpha}}{\left(\dfrac{\mu_2}{\mu_1}-1\right)}\dfrac{k_1}{k_2}\displaystyle\sum_{n=1}^{\infty}\sum_{p=1}^{\infty} q_{np,i}Y_{p1}i^{n+1}J_n(\delta_i)(-1)^n+1+\dfrac{\pi}{2}icu_1I_0, \quad r=m=1 \\ \dfrac{ze^{im\alpha}}{(m-1)!\left(\dfrac{\mu_2}{\mu_1}-1\right)}\dfrac{k_1}{k_2}2^{m-1}\displaystyle\sum_{n=1}^{\infty}\sum_{p=1}^{\infty} q_{np,i}Y_{pm}i^{n+1}J_n(m\delta_i)(-1)^n+1, \quad r=m\neq 1. \\ \dfrac{ze^{im\alpha}}{(m-1)!\left(\dfrac{\mu_2}{\mu_1}-1\right)}\dfrac{k_1}{k_2}2^{m-1}\displaystyle\sum_{n=1}^{\infty}\sum_{p=1}^{\infty} q_{np,i}Y_{pr}i^{n+r-m-1}J_n(m\delta_i)(-1)^n \quad r\neq m \end{cases} \tag{B8}$$